Freeze-in sterile neutrino dark matter in a class of U(1)′ models with inverse seesaw

Arindam Das,[1,*] Srubabati Goswami,[2,†] Vishnudath K.N.,[2,‡] and Tanmay Kumar Poddar[2,3,§]

[1] *Department of Physics, Kyungpook National University, Daegu 41566, Korea*

[2] *Theoretical Physics Division, Physical Research Laboratory, Ahmedabad - 380009, India*

[3] *Discipline of Physics, Indian Institute of Technology, Gandhinagar - 382355, India*

Abstract

We study a class of general U(1)′ models to explain the observed dark matter relic abundance and light neutrino masses. The model contains three right handed neutrinos and three gauge singlet Majorana fermions to generate the light neutrino mass via the inverse seesaw mechanism. We assign one pair of degenerate sterile neutrinos to be the dark matter candidate whose relic density is generated by the freeze-in mechanism. We consider different regimes of the masses of the dark matter particle and the Z' gauge boson. The production of the dark matter can occur at different reheating temperatures in various scenarios depending on the masses of the Z' boson and the dark matter candidate. We also note that if the mass of the sterile neutrino dark matter is $\gtrsim$ 1MeV and if the Z' is heavier than the dark matter, the decay of the dark matter candidate into positrons can explain the long standing puzzle of the galactic 511keV line in the Milky Way center observed by the INTEGRAL satellite. We constrain the model parameters from the dark matter analysis, vacuum stability and the collider searches of heavy Z' at the LHC. For the case with light Z', we also compare how far the parameter space allowed from dark matter relic density can be probed by the future lifetime frontier experiments SHiP and FASERs in the special case of $U(1)_{B-L}$ model.

* Email Address: dasarindamphysics@gmail.com

† Email Address: sruba@prl.res.in

‡ Email Address: vishnudath@prl.res.in

§ Email Address: tanmay@prl.res.in

I. INTRODUCTION

The success of the Standard Model (SM) has been consolidated by the discovery of the Higgs boson of mass ∼125GeV at the Large Hadron Collider (LHC)[1, 2]. This establishes the spontaneous symmetry breaking as the mechanism for the generation of masses of the gauge bosons and fermions except neutrinos. However, the observation of neutrino oscillations [3] in several terrestrial experiments confirm that neutrinos have tiny masses. In addition, the galaxy rotation curve and the study of the bullet cluster by the Chandra X-ray observatory along with several other astrophysical observations have demonstrated the existence of more non-luminous Dark Matter (DM) ($\sim 25\%$) in the universe than the visible matter ($\sim 5\%$) [4]. The SM does not offer any explanation to this as well. Thus, stepping beyond the SM is necessary to account for these observations.

Among different possibilities of the Beyond Standard Model (BSM) scenarios, the $U(1)'$ gauge group extensions of the SM have special significance. In this scenario, the SM is extended by an additional U(1)$'$ symmetry which requires three generations of the Right Handed Neutrinos (RHNs) to cancel all the gauge and mixed gauge-gravity anomalies [5–7]. The active light neutrinos can get mass from type-I seesaw mechanism [8, 9] after the breaking of the $U(1)'$ symmetry followed by the generation of the Majorana mass term. In canonical type-I seesaw model, one either has to go for large Majorana mass for the heavy neutrinos or very small Yukawa couplings, which makes it difficult to probe the model at the collider experiments. This motivates one to consider low-scale extensions of the canonical type-I seesaw model [10] such as the inverse seesaw model [11]. In the inverse seesaw model, the smallness of neutrino mass can be obtained from a small lepton number violating term whereas the heavy Majorana neutrinos can be at the TeV scale, thus decoupling the scales of seesaw and lepton number violation. This can allow for large light-heavy mixing, making the model testable. The $U(1)'$ scenario can also provide a potential DM candidate which can reproduce the observed relic density [12–22].

The non-observation of any signal in the direct detection DM experiments puts stringent bounds on the DM nucleon scattering cross section [23–25] which severely restrict the models with Weakly Interacting Massive Particles (WIMPs) whose masses are $\gtrsim$ 1GeV. There are

some scenarios where non-WIMP candidates such as Feebly Interacting Massive Particles (FIMPs) [26], Strongly Interacting Massive Particles (SIMPs) [27], light gauge bosons [28–30], the axions or Axion Like Particles (ALPs) [31–36], light sterile neutrinos [37], Primordial Black Holes (PBHs) [38, 39] etc., can be potential DM candidates and at the same time evading the direct detection bounds.

In this paper, we have studied a class of general $U(1)'$ models to explain the observed light neutrino mass and the relic abundance of DM. The former is generated by the inverse seesaw mechanism. Reference [20] has studied DM phenomenology in the context of this model, where, one of the heavy neutrinos with mass $\sim \mathcal{O}(\text{TeV})$ was proposed as a WIMP DM candidate with the aid of an additional Z_2 symmetry. However, in this model, strong bounds coming from the direct detection experiments resulted in predictions for DM-nucleon cross section almost close to the neutrino floor. This leads us to think of alternate non-WIMP DM candidates in these scenarios. In the present work, we assign a pair of almost degenerate pseudo-Dirac sterile neutrinos to be the potential DM candidate which are produced by the so called freeze-in mechanism [26]. In this mechanism, the initial DM abundance is negligibly small and the final DM abundance is obtained by the annihilation or decay of the SM particles. Such a DM candidate is often called as a Feebly Interacting Massive Particle (FIMP), since it couples feebly with the SM thermal radiation [26]. In this scenario, the DM yield increases with an increase in the coupling strength in contrast to the thermal freeze-out scenario [40, 41]. The freeze-in mechanism is realized in several well motivated frameworks [21, 22, 42–46]. Depending on whether the DM particles interact with the visible sector via renormalizable or non-renormalizable interactions, one can have infrared (IR) freeze-in [26, 45, 47] or ultraviolet (UV) freeze-in [26, 48–50] respectively. In the case of UV freeze-in, the DM particles are produced by scattering of the SM particles, mediated by some portal. In an effective field theory prescription, this can be described by a higher dimensional non-renormalizable operator where the cut-off scale is the mass of the mediator. In such a scenario, the production of DM dominates at relatively high temperature, greater than the masses of the scattering particles as well as of the DM (but not the mediating portal particle, since otherwise the effective field theory description will break down). On the other hand in IR freeze-in, generally the DM interacts with the visible sector via a renormalizable

operator and the production is dominated at low temperature (T down to the mass of the DM).

In this work, we study different scenarios with various limits of the Z' mass ($M_{Z'}$), DM mass (m_N) and the reheating temperature (T_R). In particular, we consider three cases : (A) $M_{Z'} \sim \mathcal{O}$(TeV) with $m_N << T_R << M_{Z'}$, (B) $M_{Z'} \sim$ 1 MeV - 100 GeV with $M_{Z'} << m_N << T_R$ and (C) $M_{Z'} \sim$ 1 MeV - 100 GeV with $m_N << M_{Z'} << T_R$. We also discuss the bounds from vacuum stability and perturbativity for the different cases. In addition, we discuss the constraints from the search for heavy Z' (case-A) at the collider experiments. For cases B and C with a light Z', we have compared the parameter space that is allowed by the DM relic density in the $M_{Z'} - g'$ plane with the regions that can be probed in the future lifetime frontier experiments such as SHiP [51] and FASERs [52, 53], for the special case of the $U(1)_{B-L}$ model. In this case, we have also incorporated the existing astrophysical bounds on the mass and coupling of a light Z'. We also note that in case-(A) with heavy Z', if the mass of the DM is $\gtrsim 1$ MeV, this scenario can explain the long standing puzzle of the galactic 511 keV line in the Milky Way center observed by the INTEGRAL satellite [54, 55], where the decay of the sterile neutrino DM into positrons can explain the observed signal. The decay of MeV scale DM to explain the 511 keV line has been studied in the context of minimal $U(1)_{B-L}$ model with type-I seesaw in [12] whereas the light Z' and DM phenomenology in the context of $U(1)'$ model by fixing the charge of one scalar with minimal seesaw has been studied in [56]. In our work, we consider the general $U(1)'$ case, but with inverse seesaw and constrain the model parameters - the new gauge coupling, the Z' mass and the $U(1)'$ charges of the two scalars from the DM analysis.

The rest of the paper is organized as follows. In Sec.-II, we describe the model and the low energy constraints in the neutrino sector. In Sec.-III, we discuss the scalar sector and the bounds on the $U(1)'$ charges of the scalars from vacuum stability and perturbativity. In Sec.-IV, we calculate the sterile neutrino DM relic density in terms of the model parameters for the three cases mentioned above. The combined bounds on the U(1)$'$ coupling and the Z' mass obtained from the DM study and other experimental searches are discussed in Sec.-V. In Sec.-VI, we have shown how the galactic 511keV line could be explained by a sterile neutrino DM of mass $\sim$ 1 MeV. Finally, we summarize our results in Sec.-VII.

	Q_{L_i}	u_{R_i}	d_{R_i}	ℓ_{L_i}	e_{R_i}	ν_{R_α}	H	Φ	S
$\mathrm{SU(3)_C}$	**3**	**3**	**3**	**1**	**1**	**1**	**1**	**1**	**1**
$\mathrm{SU(2)_L}$	**2**	**1**	**1**	**2**	**1**	**1**	**2**	**1**	**1**
$\mathrm{U(1)_Y}$	1/6	2/3	$-1/3$	$-1/2$	-1	0	1/2	0	0
$U(1)'$	$\frac{1}{6}x_h + \frac{1}{3}x_\phi$	$\frac{2}{3}x_h + \frac{1}{3}x_\phi$	$-\frac{1}{3}x_h + \frac{1}{3}x_\phi$	$-\frac{1}{2}x_h - x_\phi$	$-x_h - x_\phi$	$-x_\phi$	$\frac{1}{2}x_h$	x_ϕ	0

TABLE I: Particle content of our $U(1)'$ model. In addition to the SM fermions, we have three RHNs, ν_R and three gauge singlet fermions S. i and α are the generation indices. H is the SM Higgs doublet and Φ is the complex scalar responsible for $U(1)'$ symmetry breaking, whose $U(1)'$ charges are $\frac{1}{2}x_h$ and x_ϕ, respectively.

II. INVERSE SEESAW SCENARIO IN THE $U(1)'$ MODEL

We extend the SM gauge group $SU(3)_c \times SU(2)_L \times U(1)_Y$ by an additional $U(1)'$ symmetry. Together with the SM particle content, there is a complex scalar Φ to break the $U(1)'$ symmetry, and three RHNs ν_{Ri} and three gauge singlet Majorana fermions S_i for implementing the inverse seesaw mechanism [20]. The field content along with their transformation properties are given in TABLE. I. The gauge invariant Yukawa Lagrangian as per the charges shown in TABLE I is,

$$-\mathcal{L}_{\text{Yukawa}} = Y_e \bar{\ell_L} H e_R + Y_\nu \bar{\ell_L} \tilde{H} \nu_R + Y_u \bar{Q_L} \tilde{H} u_R + Y_d \bar{Q_L} H d_R + y_{NS} \bar{\nu_R} \Phi S + \frac{1}{2} \bar{S^c} M_\mu S + \text{h.c.}, \quad (2.1)$$

where $\tilde{H} = i\sigma_2 H^*$, h.c. denotes the Hermitian conjugate term and the generation indices are suppressed. Solving the gauge and mixed gauge-gravitational anomaly cancellation conditions, we can write the $U(1)'$ charges of all the fermions in terms of the scalar charges as shown in TABLE. I [20]. After the symmetry breaking, we obtain the neutral fermion mass terms from Eqn. (2.1) as,

$$-\mathcal{L}_{\text{mass}} = \bar{\nu_L} M_D \nu_R + \bar{\nu_R} M_R S + \frac{1}{2} \bar{S^c} M_\mu S + \text{h.c.}, \quad (2.2)$$

where, $M_D = Y_\nu \langle H \rangle$, and $M_R = y_{NS} \langle \Phi \rangle$. We can write the neutral fermion mass matrix as,

$$\mathcal{L}_{\text{mass}} = \frac{1}{2} \begin{pmatrix} \bar{\nu_L^c} & \bar{\nu_R} & \bar{S^c} \end{pmatrix} \begin{pmatrix} 0 & M_D^* & 0 \\ M_D^\dagger & 0 & M_R \\ 0 & M_R^T & M_\mu \end{pmatrix} \begin{pmatrix} \nu_L \\ \nu_R^c \\ S \end{pmatrix}, \tag{2.3}$$

where, M_D, M_R, and M_μ are 3×3 matrices and they have a mass hierarchy $M_R \gg M_D \gg M_\mu$. In this case, the effective light neutrino mass matrix becomes [11],

$$M_\nu = M_D^* (M_R^T)^{-1} M_\mu M_R^{-1} M_D^\dagger. \tag{2.4}$$

Thus, the smallness of the neutrino mass can be due to the suppression by both M_μ and $\frac{M_D}{M_R}$. The heavy neutrino sector will consist of three pairs of pseudo-Dirac neutrinos with mass $\sim M_R \pm M_\mu$. To obtain light neutrino of mass $\mathcal{O}(0.1\text{eV})$, we can take $M_\mu \sim \mathcal{O}(\text{keV})$ and $\frac{M_D}{M_R} \sim 10^{-2}$. After diagonalizing the 9×9 neutral fermion mass matrix in Eqn.2.3 [57, 58], the flavor eigenstates of the light active neutrinos (ν_α) can be expressed as a linear combination of the mass eigenstates of the light neutrinos (ν_i) and the heavy neutrinos (N_j) as,

$$\nu_\alpha = U_{\alpha i} \nu_i + V_{\alpha j} N_j, \tag{2.5}$$

where U is the Pontecorvo-Maki-Nakagawa-Sakata (PMNS) matrix and V is the 3×6 active-sterile mixing matrix. It is well known that the minimal inverse seesaw model that can explain the oscillation data requires only two ν_R and two S [59]. We use this fact and assume that only two pseudo-Dirac pairs having mass of the $\mathcal{O}(\text{TeV})$ are responsible for the light neutrino masses, making the lightest active neutrino almost massless. For the other pair of pseudo-Dirac neutrinos, which we denote by $j = 1, 2$ in Eqn. 2.5, we consider a wide range of mass in the range keV - TeV for the DM. This pair has very small values of Yukawa couplings and hence very small mixing with the active neutrinos as well as other heavy neutrinos. This satisfies the naturalness criteria since vanishing of these couplings can arise from a discrete Z_2 symmetry.

The production of the sterile neutrino DM via the so called freeze-in mechanism in different cases (corresponding to different values of $M_{Z'}$) will be discussed in detail in section-III. Within these frameworks, we have also required the values of neutrino Yukawa couplings to satisfy the following bounds:

- Constraints on the oscillation parameters (three mixing angles and two mass squared differences) as given by the global analysis with three light active neutrinos [60, 61].

- Bound on the maximum value of the sum of active light neutrino masses as given by Planck 2018 data, $\Sigma m_\nu < 0.12$ eV. [62]

- Constraints on the non-unitarity of the PMNS matrix, U from the electroweak precision observables at 90% confidence level which are given as [63],

$$|UU^\dagger| = \begin{pmatrix} 0.9979 - 0.9998 & < 10^{-5} & < 0.0021 \\ < 10^{-5} & 0.9996 - 1.0 & < 0.0008 \\ < 0.0021 & < 0.0008 & < 0.9947 - 1.0 \end{pmatrix}. \tag{2.6}$$

- Bound from lepton flavor violating decays for type-I seesaw: The corresponding branching ratio for the gold (Au) nucleus is [64], $\mathrm{Br}(\mu \text{ Au} \to \text{e Au}) < 7 \times 10^{-3}$. This is related with the parameter $\hat{R}_{e\mu}$ as [65], $\hat{R}_{e\mu} < 9.7 \times 10^{-6}$, where, $\hat{R}_{e\mu} = 2\sum_j (Y_\nu^*)_{ej}(Y_\nu)_{\mu j}\left(\frac{m_w^2}{M_j^2}\right)\ln\left(\frac{M_j}{m_w}\right)$, where j can take values $1, 2, 3$, and M_1, M_2, M_3 are the masses of the three pseudo Dirac pairs of heavy neutrinos and m_w is the mass of the W gauge boson.

- Constraints on the mixing of active neutrinos with sterile neutrino DM having a mass in the keV - MeV scale : Such a low mass sterile neutrino DM is required to have very small mixing with active light neutrinos to be consistent with the various experimental bounds that are displayed in Fig. 1. In this figure, the shaded regions are disallowed by different constraints. The region above the dotted blue line corresponds to the parameter space where the sterile neutrino is overabundant (assuming production is only via mixing). In the region above the black solid line, the sterile neutrino lifetime is shorter than the age of the universe [66]. The DM annihilation or decay in the Milky way can give rise to γ ray spectral lines that can be probed by various indirect detection experiments. These searches put constraints on the sterile neutrino DM mass and mixing parameter space. The regions above the dashed dotted cyan line, dashed red line and dash-dotted magenta line are disfavored by the search for γ spectral lines by Fermi-LAT [67], COMPTEL [68] and EGRET [68, 69] respectively. The spectral

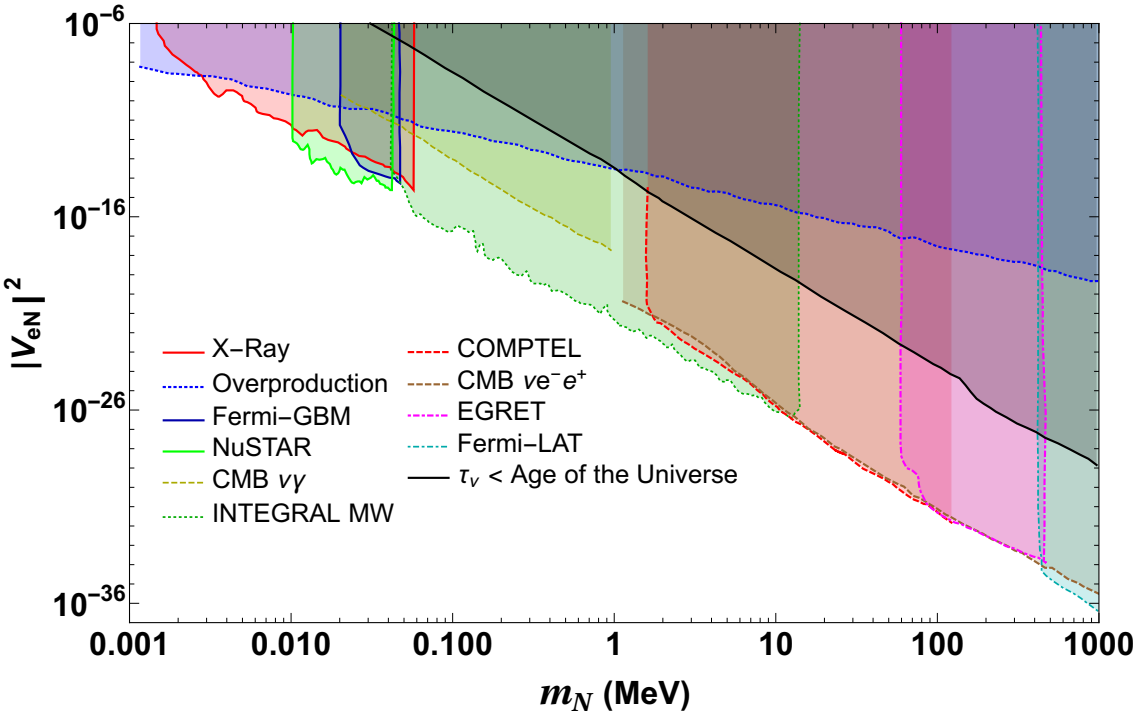

FIG. 1: Existing experimental bounds on the light heavy mixing squared ($|V_{eN}|^2$) and mass of the sterile neutrino DM. The shaded regions are disfavored by the various experiments as indicated. See main text for details.

line search by INTEGRAL MW [70] puts bound on the the active-sterile mixing for the DM of mass 0.04MeV $<$ m$_{\rm N}$ $<$ 14MeV and is shown by the region bounded by dotted green line. Searching for decaying DM of mass less than 50 keV with several X-ray telescopes put stringent bounds on the sterile neutrino mass and mixing. The region bounded by the solid red line is excluded by X-rays [37, 71–77]. The region bounded by the solid light green line is excluded by NuSTAR [78] which did not find any anomalous X-ray line from the radiative decay of sterile neutrino DM in the mass range 10keV $-$ 40keV from the galactic bulge. The region bounded by the solid blue line is excluded by Fermi-GBM [79]. The precise measurement of the cosmic microwave background (CMB) anisotropies and temperature puts constraints on the sterile neutrino DM mass and mixing. The possible decay modes of sterile neutrino are $\nu\gamma$ and $\nu e^+ e^-$ that result in early energy injection. The dashed yellow and dashed

brown lines denote the CMB constraints [80]. The decay of sterile neutrino to ν and γ gives constraints on low sterile neutrino mass (dashed yellow line) whereas the decay product $\nu e^+ e^-$ gives constraints on large sterile neutrino mass (dashed brown line). Thus, it is clear from Fig. 1 that higher the mass of the sterile neutrino DM, lower the active-sterile mixing has to be. In order to achieve this in our model, the Yukawa couplings of DM candidates to the active light neutrinos and the SM Higgs have to be very small. As mentioned earlier, we also consider a case with m_N having a mass in the $\sim \mathcal{O}$(TeV) scale, for which also we demand extremely small values of active-sterile mixing to make it stable.

In TABLE II, we have given two sample benchmark points (BM) that satisfy all the above mentioned constraints. Note that for BM-I, $M_{R11} \sim m_N \sim 1$ MeV, whereas for BM-II, $M_{R11} \sim m_N \sim 1$ TeV. Here, the lightest active neutrino is almost massless since we have assumed that the DM candidate has very small Yukawa couplings and hence do not contribute to seesaw. To generate these points, we have used the Casas-Ibarra parametrization for the inverse seesaw [81, 82], according to which, Y_ν can be written as,

$$Y_\nu = \frac{\sqrt{2}}{v} U (M_{\nu diag})^{1/2} R \; M_\mu^{-1/2} M_R^T. \tag{2.7}$$

Here, v is the vacuum expectation value (vev) of the SM Higgs boson, $M_{\nu diag}$ is the diagonal light neutrino mass matrix and R is a general orthogonal matrix which we have taken to be real for simplicity. Also, we have taken normal hierarchy (NH) for active light neutrinos, for which,

$$M_{\nu diag} = \text{diag } (m_1, \sqrt{m_1^2 + \Delta m_{sol}^2}, \sqrt{m_1^2 + \Delta m_{sol}^2 + \Delta m_{atm}^2}), \tag{2.8}$$

where $\Delta m_{sol}^2 = m_2^2 - m_1^2$ and $\Delta m_{atm}^2 = m_3^2 - m_2^2$. We have also kept the Majorana phases (α, β) to be 0 and the Dirac CP phase (δ_{CP}) to be 3.438 radian which is the best fit value for NH [60, 61]. Thus, we did a scanning with the entries of the matrices M_R, M_μ and R and m_1 as the input parameters and varied the light neutrino mass squared differences and mixing angles in the 3σ ranges to find out parameters that are consistent with all the above discussed constraints. For simplicity, we have taken both M_R and M_μ to be diagonal and real. Note that, if there was a Z_2 symmetry under which ν_{R1} and S_1 were odd, the

lightest active neutrino, ν_1 would have been massless ($m_1 = 0$). But here, we do not have the Z_2 symmetry. However, the requirement that mixing of the DM fermions with the active neutrinos have to be very small forces m_1 to take extremely small values as shown in Table-II.

III. SCALAR SECTOR AND BOUNDS FROM VACUUM STABILITY AND PERTURBATIVITY

In this section, we will discuss the bounds on the parameters x_h and x_ϕ from the stability of the electroweak vacuum and perturbativity. The $U(1)'$ scalar potential of our model is given as,

$$V(\Phi, H) = \mu_1^2(H^\dagger H) + \lambda_1(H^\dagger H)^2 + \mu_2^2(\Phi^\dagger\Phi) + \lambda_2(\Phi^\dagger\Phi)^2 + \lambda_3(\Phi^\dagger\Phi)(H^\dagger H), \tag{3.1}$$

where μ_1 and μ_2 are the mass parameters and λ_1, λ_2, and λ_3 are the quartic couplings. For the potential in Eqn. (3.1) to be stable, the trivial conditions are,

$$\lambda_1 > 0, \;\; \lambda_2 > 0 \;\text{ and, }\; \lambda_3 > 0. \tag{3.2}$$

In addition, if $\lambda_3 < 0$, the stability of the potential is satisfied if,

$$\lambda_1 > 0, \;\; \lambda_2 > 0 \;\text{ and, }\; 4\lambda_1\lambda_2 - \lambda_3^2 > 0, \tag{3.3}$$

where the potential is positive definite at large field values [83]. The *vev*s of the two scalar fields H and Φ are given by ,

$$\langle H \rangle = \frac{1}{\sqrt{2}} \begin{pmatrix} 0 \\ v \end{pmatrix} \;\text{ and }\; \langle \Phi \rangle = \frac{u}{\sqrt{2}}. \tag{3.4}$$

Together with the vacuum stability conditions, the perturbative unitarity also puts constraints on the model parameters. Considering the processes $hh \to hh$ and $\phi\phi \to \phi\phi$, one can obtain the constraints on the model parameters as [84, 85],

$$|\lambda_3| \leq 8\pi \quad \text{and} \quad 3(\lambda_1 + \lambda_2) \pm \sqrt{\lambda_3^2 + 9(\lambda_1 - \lambda_2)^2} \leq 8\pi. \tag{3.5}$$

The pertubative bounds on the gauge couplings are,

$$|g_i| \leq \sqrt{4\pi} \quad \text{and} \quad x_{q,u,d,e,\nu,l,\phi} g', \left(\frac{x_h}{2}\right) g' \leq \sqrt{4\pi}, \tag{3.6}$$

Parameter	Benchmark Point-I	Benchmark Point-II
Y_ν	$\begin{pmatrix} (1.066)10^{-17} & 0.103 - I\ 0.016 & 0.037 + I\ 0.039 \\ (-3.358 + I\ 0.381)10^{-18} & -0.149 - I\ 0.037 & 0.391 - I\ 0.028 \\ (6.686 + I\ 0.309)10^{-18} & -0.236 - I\ 0.012 & 0.141 - I\ 0.047 \end{pmatrix}$	$\begin{pmatrix} (1.221) \times 10^{-20} & 0.086 + I\ 0.003 & -0.040 + I\ 0.026 \\ (-4.812 + I\ 0.356)10^{-21} & 0.071 - I\ 0.028 & 0.251 + I\ 0.009 \\ (6.815 + I\ 0.382)10^{-21} & -0.101 - I\ 0.027 & 0.250 - I\ 0.013 \end{pmatrix}$
$Tr[Y_\nu^\dagger Y_\nu]$	0.269	0.152
M_R (GeV)	$\begin{pmatrix} 0.001 & 0 & 0 \\ 0 & 8625.978 & 0 \\ 0 & 0 & 6463.302 \end{pmatrix}$	$\begin{pmatrix} 4747.656 & 0 & 0 \\ 0 & 7005.899 & 0 \\ 0 & 0 & 4095.693 \end{pmatrix}$
M_μ (GeV)	$\begin{pmatrix} 1.945 \times 10^{-8} & 0 & 0 \\ 0 & 8.660 \times 10^{-7} & 0 \\ 0 & 0 & 2.302 \times 10^{-7} \end{pmatrix}$	$\begin{pmatrix} 3.401 \times 10^{-7} & 0 & 0 \\ 0 & 6.850 \times 10^{-7} & 0 \\ 0 & 0 & 2.159 \times 10^{-7} \end{pmatrix}$
δ_{CP}	3.438	3.438
α, β	$0, 0$	$0, 0$
m_{light} (eV)	$10^{-22}, 8.476 \times 10^{-3}, 5.056 \times 10^{-2}$	$10^{-40}, 8.802 \times 10^{-3}, 4.955 \times 10^{-2}$
$\Sigma_\alpha \lvert V_{\alpha 1}\rvert^2$	2.570×10^{-24}	1.470×10^{-43}

TABLE II: The sample benchmark points for the neutrino parameters that satisfy all the experimental bounds as discussed in the main text. Note that here, $M_R = \frac{y_{NS} u}{\sqrt{2}}$.

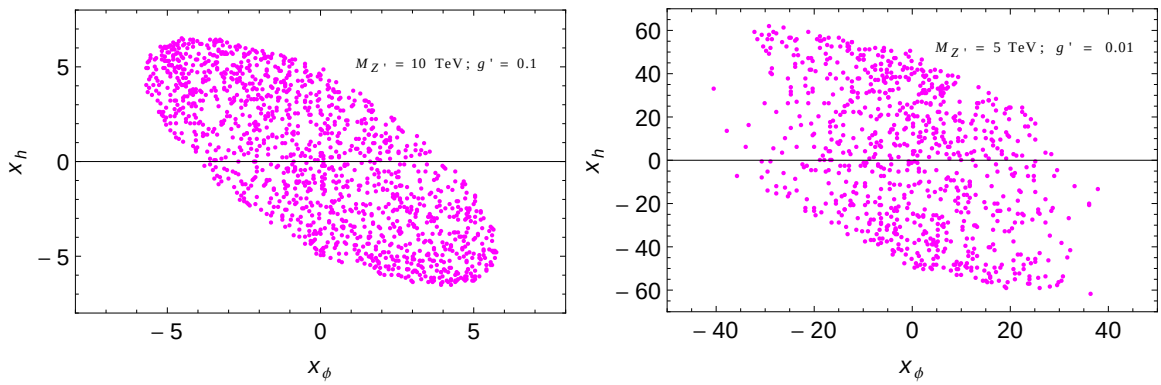

FIG. 2: Parameter space allowed by vacuum stability and perturbativity constraints in the $x_\phi - x_h$ plane. The left panel is for $M_{Z'} = 10$ TeV and $g' = 0.1$ whereas the right panel is for $M_{Z'} = 5$ TeV and $g' = 0.01$.

respectively. Here, g_i with $i = 1, 2, 3$ correspond to the SM hypercharge, weak and strong gauge couplings respectively whereas g' is the $U(1)'$ gauge coupling. The vacuum stability and perturbativity bounds for the $U(1)'$ motivated inverse seesaw scenario has been extensively studied in [20]. In Fig. 2, we have shown the parameter space allowed by vacuum stability and perturbativity constraints in the $x_\phi - x_h$ plane. The left panel is for $M_{Z'} = 10$ TeV and $g' = 0.1$ whereas the right panel is for $M_{Z'} = 5$ TeV and $g' = 0.01$. Similar constraints in the $x_\phi - x_h$ parameter space have been obtained in [20], but for fixed values of m_{h_2}, θ and u, where m_{h_2} is the mass of the heavy physical Higgs scalar and θ is its mixing angle with the SM Higgs. The expressions for m_{h_2} and θ and the tree level matching conditions for the scalar quartic couplings are given in section-III of [20]. In Fig. 2, we have varied m_{h_2} in the range $0.5 - 15$ TeV and θ in the range $0 - 1$ for both the panels. Also, keeping $M_{Z'}$ and g' fixed and varying x_ϕ would mean that the *vev* of ϕ, u has to be varied as per the relation $u = \frac{M_{Z'}}{|x_\phi| g'}$. For the neutrino Yukawa couplings, we have used the benchmark point-I in TABLE II.

In plotting Figs. 2 and 3, we have used the mass of the SM Higgs boson, $m_{h_1} = 125.6$ GeV, mass of the top quark, $M_t = 173.4$ GeV and the strong coupling constant, $\alpha_s = 0.1184$ and calculated all the SM couplings at the top mass scale (M_t) after taking into the threshold corrections [86–88], and then run them from (M_t) to the scale u using SM RGEs. At the

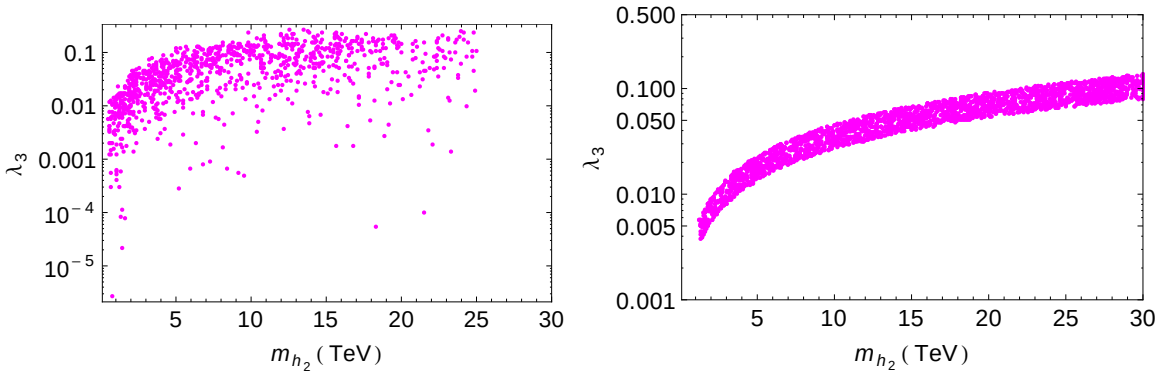

FIG. 3: Parameter space allowed by vacuum stability and perturbativity constraints in the $\lambda_3 - m_{h_2}$ plane. The left panel is for $g' = 0.1, M_{Z'} = 1$ TeV whereas the right panel is for $g' = 10^{-6}, M_{Z'} = 10$ MeV.

scale u, the new $U(1)'$ couplings also enter into the RGE running. The modified RGEs for our model are generated by SARAH [89]. We have used two loop RGEs for the SM parameters and one loop RGEs for all the BSM couplings. They are given in the appendix of reference [20]. From Fig. 2, we can see that for $M_{Z'} = 10$ TeV and $g' = 0.1$, the allowed values of x_ϕ and x_h are in the ranges ~ -5.7 to $+5.7$ and ~ -6.5 to $+6.5$ respectively. On the other hand, for $M_{Z'} = 5$ TeV and $g' = 0.01$, large values of x_ϕ and x_h are allowed with $-40 \lesssim x_\phi \lesssim +38$ and $-59 \lesssim x_h \lesssim 62$. This is expected from Eq. 3.6 since the perturbativity conditions are on the products of x_h and x_ϕ with g', thus allowing larger values of x_h and x_ϕ for smaller values of g'.

In Fig.3, we have plotted the allowed values of λ_3 against m_{h_2} that satisfy the vacuum stability as well as perturbativity constraints. The left panel is for $g' = 0.1, M_{Z'} = 1$ TeV whereas the right panel is for $g' = 10^{-6}, M_{Z'} = 10$ MeV. Also, for the left panel, we have varied x_h and x_ϕ in the range -10 to 10 and for the right panel, they are varied in the range -1000 to +1000. From this plot, we can see that the values of λ_3 as low as 2×10^{-6} are allowed for $g' = 0.1$. On the other hand, for $g' = 10^{-6}$, values of $\lambda_3 < 0.003$ are disfavored by the bounds from absolute stability. In fact, both λ_3 and g' affect the stability of the electroweak vacuum positively. This is why much lower values of λ_3 are allowed for higher values of g'. At this point, it is worth mentioning that demanding the electroweak vacuum

to be absolutely stable puts rather stringent bounds. This can be relaxed by allowing the vacuum to be metastable. It is known that the electroweak vacuum is metastable in the SM for the central values of the parameters [90, 91]. Once the electroweak vacuum is allowed to be metastable in the $U(1)'$ model, even smaller values of λ_3 can be allowed by taking small values of the neutrino Yukawa couplings [92]. In fact taking extremely small values of λ_3, g' and neutrino Yukawa couplings would give almost the same RGEs as in the SM where the vacuum is mostly metastable depending on the values of the parameters chosen.

IV. STERILE NEUTRINO DM

In this section, we discuss in detail about the non-thermal production of the sterile neutrino DM via the freeze-in mechanism for different regimes of $M_{Z'}$. We calculate the DM relic density in each case and constrain the model parameters by requiring the sterile neutrino DM candidate to account for the entire relic abundance of the universe. Particularly, we consider three cases : (A) $m_N << T_R << M_{Z'}$ with $M_{Z'} \sim \mathcal{O}$(TeV), $m_N \sim$ 10 keV - 10 MeV and $T_R \sim$ 5 - 100 MeV , (B) $M_{Z'} << m_N << T_R$ with $M_{Z'} \sim$ 0.1 MeV - 100 GeV, $m_N \sim \mathcal{O}$(TeV) and $T_R >>$ TeV and (C) $m_N << M_{Z'} << T_R$ with $M_{Z'} \sim$ 0.1 MeV - 100 GeV, $m_N \sim$ 10 keV - 10 MeV and $T_R >>$ TeV [1]. Here, cases (A) and (C) have relatively lighter sterile neutrinos as the DM candidate, depending upon $M_{Z'}$ and T_R. A light sterile neutrino of mass in the $\sim$ keV - MeV range cannot be a thermal relic in this model, since it will become a hot DM because of the gauge interaction with the heavy Z' boson [40, 93]. One way to produce sterile DM is from active-sterile oscillation by the so called Dodelson-Widrow (DW) mechanism [94]. However, the large active-sterile mixing required for the DW mechanism to work is in strong tension from the x-ray observations as we have seen in Fig. 1. In addition, the warmness of the DM produced by the DW mechanism disrupts the small scale structures which is constrained by the Lyman-α measurements [95–97]. Hence, the x-ray and Lyman-α

[1] In standard inflationary models, the radiation dominated era is believed to start with the decay of coherent oscillation of a scalar field and the decay products are thermalized into the thermal bath with a temperature called the reheating temperature, T_R [40]. At high T_R, the particles remain in thermal equilibrium and the entropy is conserved after they decouple. However, we do not have any physical evidence of radiation dominated era before the epoch of big bang nucleosynthesis (BBN) which roughly occurs at $T \sim$ 1MeV. So one can choose low values of T_R around 1 MeV or values as large as 10^{16} GeV.

constraints rule out this mechanism as a possible way of producing the sterile neutrino DM. There are other mechanisms in the literature which can produce sterile neutrino DM. The Shi-Fuller mechanism [98] resonantly produce sterile neutrinos from active sterile oscillation which requires a large lepton asymmetry. This mechanism produces cold DM. However, this scenario has stringent constraints from structure formation [99, 100]. Hence, we consider the non-thermal production of sterile neutrino DM relic abundance by freeze-in process. In this scenario, the initial number density of the DM is very small and the abundance builds up by interaction with the SM thermal bath. But the interaction rate is assumed to be small enough so that the DM particles do not attain thermal equilibrium with the bath. Therefore, the DM annihilation to the SM particles can be ignored. In the $U(1)'$ model that we are considering, the DM particles are produced by the annihilation of the SM particles mediated by the Z' gauge boson. This is shown in Fig. 4. As discussed earlier, we have a pair of almost degenerate pseudo-Dirac neutrinos that act as the DM. The corresponding mass terms are given as,

$$-\mathcal{L}_{DMmass} \sim \frac{1}{2}\begin{pmatrix}\bar{\nu_{R1}} & \bar{S^c}_1\end{pmatrix}\begin{pmatrix}0 & M_{R11}\\ M_{R11} & M_{\mu 11}\end{pmatrix}\begin{pmatrix}\nu^c_{R1}\\ S_1\end{pmatrix}. \tag{4.1}$$

The corresponding mass eigenvalues are $M_{R11} \pm M_{\mu 11} \sim M_{R11} \sim m_N$, since $M_{\mu 11} << M_{R11}$. In this limit, the above matrix can be diagonalized by,

$$U_{DM} \sim \frac{1}{\sqrt{2}}\begin{pmatrix}i & 1\\ -i & 1\end{pmatrix}. \tag{4.2}$$

The interaction of the Z' with the DM is given as,

$$-\mathcal{L} \sim g' Q_\nu Z'^\mu (\bar{\nu_R})_1 \gamma_\mu (\nu_R)_1, \tag{4.3}$$

where $Q_\nu = -x_\phi$. Similarly, for the SM fermions, the Z' interaction has the form,

$$-\mathcal{L} \sim g' Q_L Z'^\mu \bar{f}_L \gamma_\mu f_L + g' Q_R Z'^\mu \bar{f}_R \gamma_\mu f_R, \tag{4.4}$$

with Q_L and Q_R being the $U(1)'$ charges of the left and right chiral fermions.

The relic abundance of the DM is calculated by solving the Boltzmann equation, which is given as,

$$\dot{n} + 3Hn =< \sigma v(ab \to NN) > n_a n_b, \tag{4.5}$$

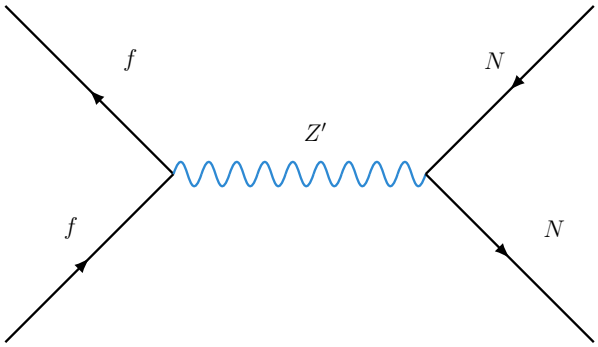

FIG. 4: Feynman diagram showing the production of sterile neutrino DM from scattering of SM fermions mediated by Z' gauge boson.

where n is the number density of the sterile neutrino DM, a and b are the initial state particles, and $< \sigma v >$ is the thermal average product of the cross section and the relative velocity of the initial state particles.

A. Heavy Z' ($M'_Z \gg T_R \gg m_N$)

In this case, we assume one pair of the sterile neutrinos to have mass in the keV-MeV range to be the DM candidates and $M_{Z'} \sim \mathcal{O}(\text{TeV})$. Here we have chosen the reheating temperature (T_R) to be relatively low, in the range $5 - 100$ MeV. Hence, the relevant initial state particles (whose masses are less than T_R) for the production of the DM are electron-positron ($e^- e^+$) and neutrino-anti neutrino ($\nu\bar{\nu}$) pairs, whose scatterings mediated by the heavy Z' will produce the DM. Note that in this scenario, we take the Z' portal coupling to the DM particle (i.e., the $U(1)'$ gauge coupling) to be relatively large, $g' \sim \mathcal{O}(0.1)$ corresponding to $M_{Z'} \sim \mathcal{O}(\text{TeV})$, unlike the usual freeze-in scenarios where the portal couplings are taken to be very small. This is possible since we are considering low T_R so that there will not be any overproduction of the DM. To calculate the relic abundance, the Boltzmann equation (Eqn. 4.5) has to be solved. The collision term in the Boltzmann equation, i.e., the right hand side of Eqn. 4.5 can be written as,

$$< \sigma v(ab \to NN) > n_a n_b = \frac{4T^4}{(2\pi)^5} \int_{\frac{2m_N}{T}}^{\infty} dx x^2 K_1(x) \sum_{a,b} g_a g_b \mathcal{F}(x^2 T^2, ab \to NN), \qquad (4.6)$$

where $x = \sqrt{s}/T$ with s being the Mandelstam variable, g_i stands for the internal degrees of freedom and $K_1(x)$ is the first order modified Bessel function of the second kind and $\mathcal{F}(s)$ is given as,

$$\mathcal{F}(s, ab \to NN) = \frac{1}{32\pi} \int \frac{d\cos\theta}{2} \sqrt{\frac{s - 4m_i^2}{s}} |\bar{\mathcal{M}}_{ab}(s, \cos\theta)|^2, \tag{4.7}$$

where m_i is the mass of the initial state particles. We calculate the spin averaged amplitude square for the process $f\overline{f} \to NN$ in the s-channel mediated by the Z' as,

$$|\bar{\mathcal{M}}|^2 = \frac{{g'}^4 {y'_N}^2}{(k^2 - M_{Z'}^2)^2 + M_{Z'}^2 \Gamma_{Z'}^2} \Big[c_V^2 \{ s^2 + (s - 4m_f^2)(s - 4m_N^2)\cos^2\theta - 4s(m_N^2 - m_f^2) - 16 m_N^2 m_f^2 \}$$
$$+ c_A^2 \{ s^2 + (s - 4m_f^2)(s - 4m_N^2)\cos^2\theta - 4s(m_N^2 + m_f^2) + 16 m_N^2 m_f^2 + \frac{16 m_f^2 m_N^2}{M_{Z'}^4}(s - M_{Z'}^2)^2 \} \Big], \tag{4.8}$$

where m_f is the mass of the fermion, m_N is the mass of the sterile neutrino DM, $y'_N = -x_\phi$ denotes the $U(1)'$ charge of the DM, s is the Mandelstam variable, θ is the scattering angle in the centre of mass frame, and c_V and c_A are the vector and axial vector couplings that depend on the $U(1)'$ charges.

When T_R is several MeV , the relevant initial states are $e^- e^+$ and $\nu\bar{\nu}$. Introducing the comoving number density $Y = n/\mathcal{S}$ where $\mathcal{S}$ is the entropy density, the final abundance of the DM is,

$$Y_\infty = \int^{T_R} \frac{< \sigma v(ab \to NN) > n_a n_b}{\mathcal{S} H T} dT, \tag{4.9}$$

where the Hubble parameter is defined as $H(T) = 1.66\sqrt{g_*}\frac{T^2}{M_{pl}}$ in the radiation dominated era and the entropy density can be written as $\mathcal{S}(T) = \frac{2\pi^2}{45} g_* T^3$. Here, M_{pl} is the reduced Planck mass and g_* is the total number of effective massless degrees of freedom ($m_i \ll T$). The c_V and c_A coefficients for the electron can be expressed in terms of the $U(1)'$ charges as, $c_V = -\frac{3}{4}x_h - x_\phi$ and $c_A = \frac{x_h}{4}$ allowing us to write,

$$\int \frac{d\cos\theta}{2} |\bar{\mathcal{M}}_{e^+e^-}(s, \cos\theta)|^2 = \frac{{g'}^4 {y'_N}^2}{(k^2 - M_{Z'}^2)^2 + M_{Z'}^2 \Gamma_{Z'}^2} \times \frac{4}{3} \Big[\Big(\frac{3}{4} x_h + x_\phi \Big)^2 (s - 4m_N^2)(s + 2m_e^2)$$
$$+ \Big(\frac{x_h}{4} \Big)^2 \{ (s - 4m_N^2)(s - 4m_e^2) + \frac{12 m_N^2 m_e^2}{M_{Z'}^4}(s - M_{Z'}^2)^2 \} \Big]. \tag{4.10}$$

The c_V and c_A for the neutrinos in terms of the $U(1)'$ charges can be written as $c_V = -x_\phi - \frac{x_h}{4}$, $c_A = -\frac{x_h}{4}$, using which we can write,

$$\int \frac{d\cos\theta}{2}|\bar{\mathcal{M}}_{\nu\bar{\nu}}(s,\cos\theta)|^2 = \frac{g'^4 {y'_N}^2}{(k^2-M_{Z'}^2)^2+M_{Z'}^2\Gamma_{Z'}^2} \times \frac{2}{3}\Big[\Big(\frac{1}{4}x_h + x_\phi\Big)^2(s-4m_N^2)(s+2m_\nu^2) + \Big(\frac{x_h}{4}\Big)^2\{(s-4m_N^2)(s-4m_\nu^2) + \frac{12m_N^2m_\nu^2}{M_{Z'}^4}(s-M_{Z'}^2)^2\}\Big]. \tag{4.11}$$

In writing the amplitude in Eqn. 4.11, we have neglected the contribution of the diagram with the active-sterile mixing since it is suppressed. The intermediate scalar contributions are also suppressed due to the small Yukawa couplings of the sterile neutrino DM and can be safely neglected.

We can write g_* as,

$$g_*(T) = \sum_{i=boson} g_i\Big(\frac{T_i}{T}\Big)^4 + \frac{7}{8}\sum_{i=fermion} g_i\Big(\frac{T_i}{T}\Big)^4. \tag{4.12}$$

If $T \ll$ MeV, the three species of the light neutrinos together with the photon are the only relativistic degrees of freedom. The neutrino temperature T_ν is related to the photon temperature T_γ by $T_\nu = \Big(\frac{4}{11}\Big)^{\frac{1}{3}} T_\gamma$ and we get, $g_*(T \ll \text{MeV}) = 3.4$. For 100 MeV $\gtrsim$ T $\gtrsim$ 1 MeV, the electron and positron are the additional degrees of freedom and the temperature of the neutrino and the photon are equal. Hence in this regime, we obtain $g_* = 10.75$. In the massless limit of the initial state particles and $M_{Z'} \gg T_R \gg m_N$, Eqn. 4.9 becomes,

$$Y_\infty \simeq 1.16\times10^{-7} \times \Big(\frac{10}{g_*}\Big)^{\frac{3}{2}}\Big(\frac{T_R}{5\text{MeV}}\Big)^3\Big(\frac{9.7\text{TeV}}{M_{Z'}/g'}\Big)^4 \times x_\phi^2\Big[2\Big\{\Big(\frac{3}{4}x_h+x_\phi\Big)^2+\Big(\frac{x_h}{4}\Big)^2\Big\} + \Big\{\Big(x_\phi+\frac{x_h}{4}\Big)^2+\Big(\frac{x_h}{4}\Big)^2\Big\}\Big]. \tag{4.13}$$

The center of mass energy in the process is such that $m_f^2 \ll s$ where f denotes all the fermions in the process. The density parameter for the DM is given by $\Omega_N = \frac{\rho}{\rho_c}$, where $\rho_c = \frac{3H_0^2}{8\pi G} = 1.05\times10^{-5}h^2\text{GeV/cm}^3$, h is the reduced Hubble constant and $\rho = m_N\mathcal{S}_0Y_\infty$ with $\mathcal{S}_0 = 2889.2\text{cm}^{-3}$. Hence, the abundance of the DM becomes,

$$\Omega_N h^2 \simeq 0.12 \times \Big(\frac{m_N}{1\text{MeV}}\Big)\Big(\frac{10}{g_*}\Big)^{\frac{3}{2}}\Big(\frac{T_R}{5\text{MeV}}\Big)^3\Big(\frac{9.7\text{TeV}}{M_{Z'}/g'}\Big)^4 \times \frac{x_\phi^2}{3}\Big[2\Big\{\Big(\frac{3}{4}x_h+x_\phi\Big)^2+\Big(\frac{x_h}{4}\Big)^2\Big\} + \Big\{\Big(x_\phi+\frac{x_h}{4}\Big)^2+\Big(\frac{x_h}{4}\Big)^2\Big\}\Big]. \tag{4.14}$$

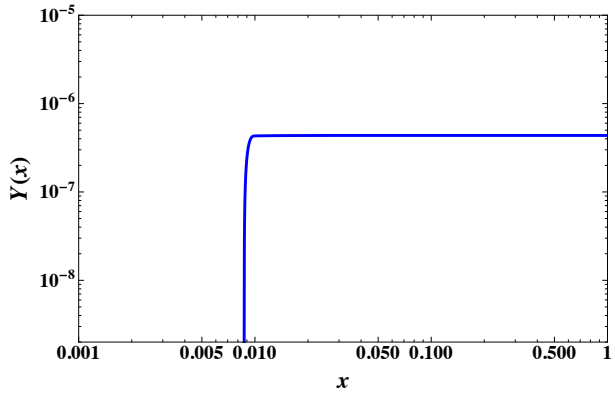

FIG. 5: Variation of the DM yield with $x = \frac{m_N}{T}$ for case-A. We have fixed $m_N = 1\text{MeV}$, $g' = 0.0827$, $M_{Z'} = 10\text{TeV}$, $T_R = 100\text{MeV}$, $x_h = -1.2$, and $x_\phi = 1$.

From the above equation, we can see that the relic density of the DM depends on the mass of the DM (m_N), the reheating temperature (T_R), the ratio $M_{Z'}/g'$ and the $U(1)'$ charges of H and Φ. Particularly, the relic density of the DM is proportional to its mass. Also, the relic density increases with the increase of x_h and x_ϕ for fixed values of other parameters.

In Fig.5, we have shown the variation of the DM yield (Y) with m_N/T by numerically solving the Boltzmann equation. In plotting this, we have fixed $m_N = 1\text{MeV}$, $g' = 0.0827$, $M_{Z'} = 10\text{TeV}$, $T_R = 100\text{MeV}$, $x_h = -1.2$, and $x_\phi = 1$, and the resultant $Y_\infty = 4.36 \times 10^{-7}$ gives the correct relic density. We can see that the freeze-in of the DM particles occurs at $T = T_R = 100$ MeV.

In FIG. 6, we have shown the relic density plot in the $x_h - x_\phi$ plane. In the left panel, we have fixed the values of the parameters as $m_N = 1$ MeV, $T_R = 10$ MeV, $M_{Z'} = 10$ TeV and $g' = 0.1$ whereas the right panel is for $m_N = 10$ MeV, $T_R = 50$ MeV, $M_{Z'} = 5$ TeV and $g' = 0.01$. Here, the white regions are disfavored by the overabundance of the DM whereas it is under abundant in the black regions. One can see that if we demand the sterile neutrinos to account for the entire DM relic abundance, there exists stringent bounds on the allowed values of x_ϕ for a given set of parameters whereas for x_h, a wide range of values ranging from -10 to 10 are allowed. Specifically, only values of $x_\phi \sim 5$ to 6 and $x_\phi \sim -5$ to -6 for the left panel, and $x_\phi \sim 4$ to 5 and $x_\phi \sim -4$ to -5 for the right panel can account for the total DM relic abundance for the chosen set of parameters. As we have seen from Fig. 2, these x_ϕ

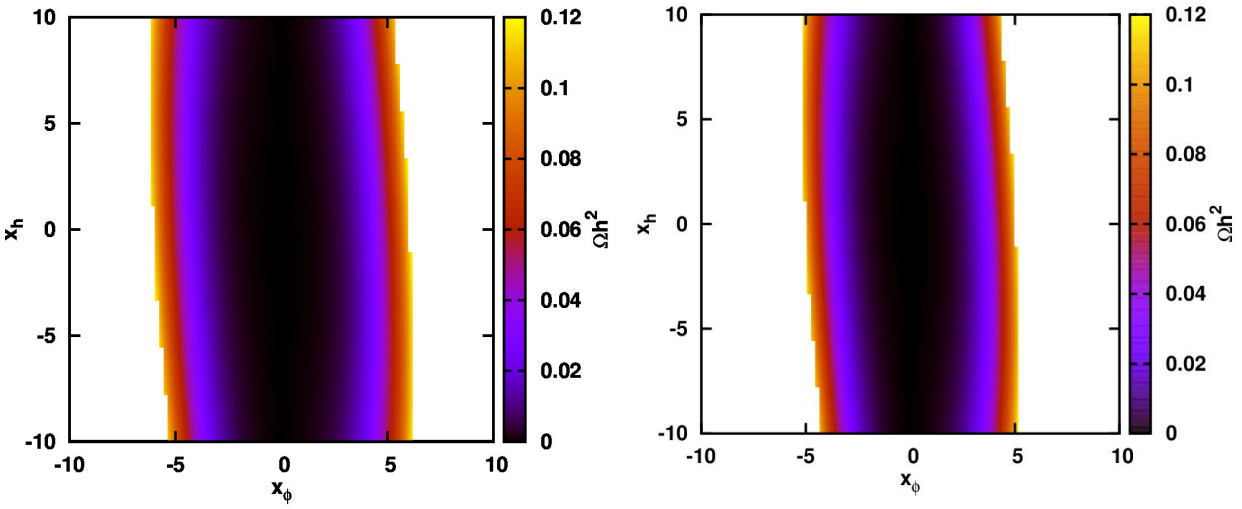

FIG. 6: Relic density plot in the $x_h - x_\phi$ plane for case-A discussed in the text. In the left panel, we have fixed the values of the parameters as $m_N = 1$ MeV, $T_R = 10$ MeV, $M_{Z'} = 10$ TeV and $g' = 0.1$ whereas the right panel is for $m_N = 10$ MeV, $T_R = 50$ MeV, $M_{Z'} = 5$ TeV and $g' = 0.01$.

values are also allowed by the vacuum stability and perturbativity bounds whereas some of the x_h values are disfavored by perturbativity in the left panel of Fig. 6 (where $g' = 0.1$).

In Fig. 7, we have shown the variation of the DM relic density with the DM mass, m_N and the reheating temperature, T_R. The values of the parameters g' and $M_{Z'}$ are fixed to be 0.1 and 10 TeV respectively, in both the plots. The left panel is plotted for $x_h = 1$ and $x_\phi = 1$ whereas the right panel is for $x_h = -5$ and $x_\phi = 5$. Note that these chosen values of x_h and x_ϕ are also consistent with the vacuum stability and perturbativity bounds which we have seen from Fig. 2. In both the panels, the white region is disfavored by the overabundance of the DM relic density. From these two figures, we can see that with the increase in m_N and T_R, the relic density increases as is expected from Eq. 4.14. For $x_h = 1$ and $x_\phi = 1$, the minimum value of m_N that gives the correct relic abundance is 0.6 MeV corresponding to $T_R = 100$ MeV. On the other hand, for $x_h = -5$ and $x_\phi = 5$, one can obtain the correct DM relic abundance for the values of m_N as low as 10 keV corresponding to $T_R \sim 82$ MeV. But in this case, the maximum value of m_N allowed is ~ 0.3 MeVfor $T_R \sim 30$ MeV. This behaviour is expected since from Eqn.4.14, we have seen that higher values of x_h and x_ϕ give

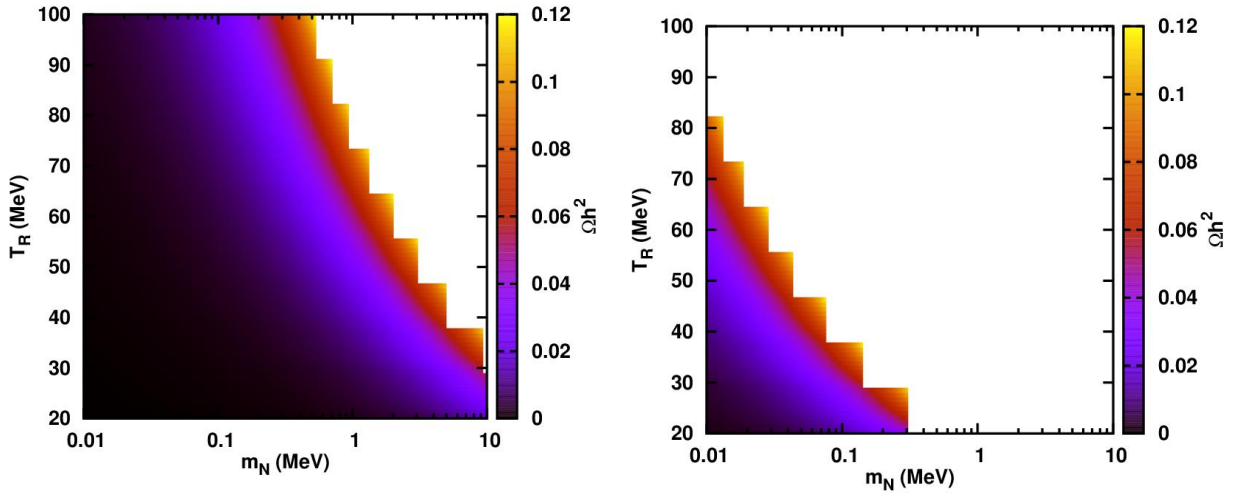

FIG. 7: Variation of relic density of DM with the mass of the DM, m_N and the reheating temperature, T_R for case-A discussed in the text. The values of the parameters g' and $M_{Z'}$ are fixed to be 0.1 and 10 TeV in both the plots. The left panel is plotted for $x_h = 1$ and $x_\phi = 1$ whereas the right panel is for $x_h = -5$ and $x_\phi = 5$.

more relic abundance and thereby disallowing higher values of m_N and T_R.

Note that even though we have restricted ourselves to low T_R in this particlar scenario, it is also possible to have values of T_R as high as $\mathcal{O}$(TeV), the only requirement being that $M_{Z'} > T_R$ so that the effective field theory description will work. For instance, when $M_{Z'} = 10$TeV and $T_R = 1$TeV, all the SM particles are involved in the scattering process. Thus we have to choose a small value of g' to prevent overabundance of the DM relic density. As an example, when $x_h = 1, x_\phi = 1$ and $m_N = 1$MeV, the correct DM relic density can be obtained by taking $g' \sim 1.49 \times 10^{-4}$. Also, note that such low values of g' are not constrained by collider experiments as well as we will see later in Fig. 17.

In Fig. 8 we have shown the variation of the relic density of the DM with $M_{Z'}$. In both the figures, we have fixed the parameters m_N, g' and T_R as 1 MeV, 0.1 and 5 MeV respectively. The dashed green line denotes $\Omega_N h^2 = 0.12$, above which, the parameter space is disallowed by the overabundance of the DM relic density. In the left panel, the red, blue, green and cyan lines are plotted for the values of $(x_h, x_\phi) = (1, 1)$, $(5, 1)$, $(1, 5)$ and $(5, 5)$ respectively. In the right panel, the red, blue, green and cyan lines denote $(x_h, x_\phi) = (-1, 1)$, $(-1, 5)$, $(-5, 1)$ and

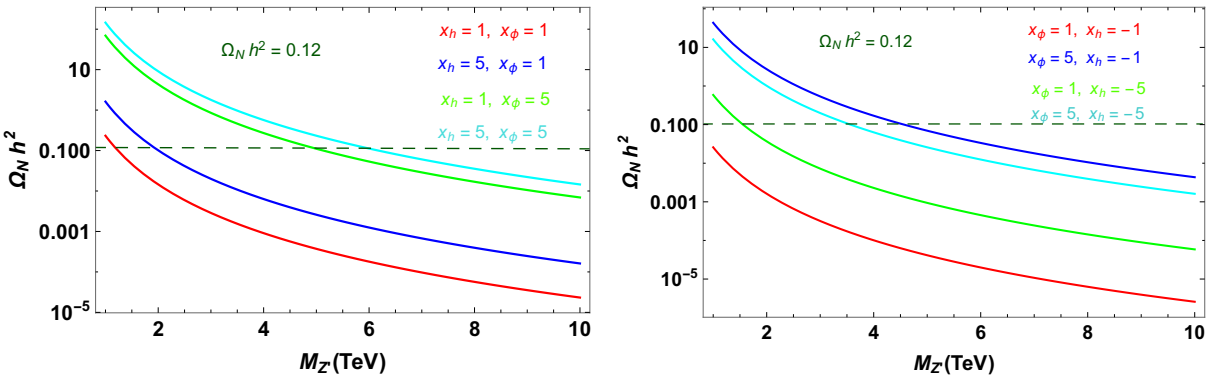

FIG. 8: Variation of the DM relic density with the mass of Z' for case-A discussed in the text. We have fixed the parameters m_N, g' and T_R as 1 MeV, 0.1 and 5 MeV respectively for both the plots. The dashed green line denotes $\Omega_N h^2 = 0.12$, above which, the parameter space is disallowed by the overabundance of the DM relic density. In the left panel, the red, blue, green and cyan lines are plotted for the values of $(x_h, x_\phi) = (1, 1)$, $(5, 1)$, $(1, 5)$ and $(5, 5)$ respectively. In the right panel, the red, blue, green and cyan lines denote $(x_h, x_\phi) = (-1, 1)$, $(-1, 5)$, $(-5, 1)$ and $(-5, 5)$ respectively.

$(-5, 5)$ respectively. From both the figures, we can see that the relic density decreases with the increase in the mass of Z'. This can be understood from Eqn.4.14, according to which $\Omega_N h^2 \propto \frac{1}{M_{Z'}^4}$. Also, higher values of x_h and x_ϕ give larger values of the DM relic density. Thus, by increasing M'_Z, one can accommodate large values of x_h and x_ϕ to reproduce the observed DM relic density consistently.

B. Light Z' ($M'_Z \ll m_N \ll T_R$)

Now we consider the case where the DM portal interaction is mediated by a light Z' with the mass of the sterile neutrino DM, m_N much greater than M'_Z. Particularly, we keep $M_{Z'}$ in the range 0.1MeV $\lesssim M_{Z'} \lesssim$ 1GeV and $m_N \gg M_{Z'}$. Also, we assume that the DM is produced non-thermally via freeze-in only by scatterings mediated by Z' (Fig. 4) and not by scalar mediated diagrams. For this, we keep the scalar mixing parameter λ_3 to be very small ($\lambda_3 \lesssim 10^{-6}$) and the mass of the extra scalar to be very large [42, 43, 101, 102]. The DM production practically stops from the thermal plasma when the temperature becomes

smaller than twice the DM mass from kinematics. In this limit, we can neglect $M_{Z'}$ and $\Gamma_{Z'}$ in the denominator of Eqn.4.8 and the cross section in the context of high T_R becomes,

$$\sigma(s) = \frac{1}{48\pi}\frac{g'^4 s\Big(1-\frac{4m_N^2}{s}\Big)^{\frac{3}{2}}}{s^2}x_\phi^2(10x_h^2+13x_\phi^2+16x_h x_\phi). \tag{4.15}$$

For high temperature ($T \gtrsim 300$GeV), all the SM particles including the three generations of quarks and leptons, eight gluons, $W\pm, Z^0$, and the Higgs doublet are relativistic, and the total relativistic degrees of freedom becomes $g_* = 106.75$. The initial condition for the production of DM by freeze-in mechanism is $Y(x_i) = 0$ for $x_i \ll 1$ and the coupling between the DM and SM particles is very small. Hence, for $x \lesssim 1$, the Boltzmann equation becomes,

$$\frac{dY}{dx} \simeq \frac{\mathcal{S}(m_N)}{H(m_N)}\frac{<\sigma v>}{x^2}Y_{EQ}^2, \tag{4.16}$$

or,

$$\frac{dY}{dx} \simeq \frac{2.8}{g_*^{\frac{3}{2}}}M_{pl}m_N\frac{<\sigma v>}{x^2}, \tag{4.17}$$

where $\mathcal{S}(m_N)$ and $H(m_N)$ are entropy density and the Hubble parameter at $T = m_N$ respectively. Y_{EQ} is the DM yield in thermal equilibrium and $n_{eq} = \frac{g_N m_N^3}{2\pi^2 x}K_2(x)$, where $K_2(x)$ is the modified Bessel function of the second kind and $g_N = 2$ is the degree of freedom of Majorana sterile neutrino DM. The thermal average DM annihilation cross section can be written as,

$$<\sigma v> = \frac{1}{(n_{eq})^2}g_N^2\frac{m_N}{64\pi^2 x}\int_{4m_N^2}^{\infty} ds \times 2(s-4m_N^2)\sigma(s)\sqrt{s}K_1\Big(\frac{\sqrt{s}}{T}\Big). \tag{4.18}$$

If the DM production is mediated by light Z' and $m_N \gg M'_Z$ then for $x \lesssim 1$, Eqn. 4.18 becomes,

$$<\sigma v> \simeq \frac{g'^4}{384\pi}\frac{x^2}{m_N^2}x_\phi^2(10x_h^2+13x_\phi^2+16x_h x_\phi). \tag{4.19}$$

Since, the production of the DM particle from thermal plasma stops at $x \sim 1$ (i.e., $T \sim m_N$), the DM yield is approximated as $Y_\infty = Y(x=1)$. Putting the expression of Eqn. 4.19 in the Boltzmann equation shown (Eqn. 4.17) and integrating from $x_i \ll 1$ to $x = 1$, we obtain,

$$Y_\infty \simeq 2.32\times 10^{-3}\frac{g'^4}{g_*^{\frac{3}{2}}}\frac{M_{pl}}{m_N}x_\phi^2(10x_h^2+13x_\phi^2+16x_h x_\phi) \quad \text{at} \quad T \sim m_N. \tag{4.20}$$

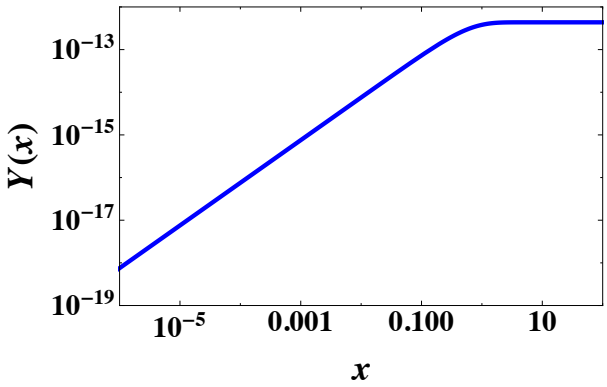

FIG. 9: Variation of the DM yield with $x = \frac{m_N}{T}$ for case-B. Here we have chosen $m_N = 1\text{TeV}$, $M_{Z'} = 0.1\text{GeV}$, $x_h = -1.2$, $x_\phi = 1$ and $g' = 3.65 \times 10^{-6}$.

Hence, the comoving yield of the sterile neutrino DM is inversely proportional to its mass. We can write the relic density of m_N as,

$$\Omega_N h^2 = \frac{m_N Y_\infty \mathcal{S}_0}{\frac{\rho_c}{h^2}} = 0.12 \times \left(\frac{106.75}{g_*}\right)^{\frac{3}{2}} \left(\frac{g'}{3.04 \times 10^{-6}}\right)^4 x_\phi^2 (10x_h^2 + 13x_\phi^2 + 16x_h x_\phi). \quad (4.21)$$

This is the relic density of DM in $m_N \gg M_{Z'}$ limit. The relic density increases with the fourth power of the Z' coupling and the $U(1)'$ charges of the scalars whereas it is independent of the masses of the Z' and the DM candidate as well as T_R. This is in contrast with the case of the heavy mediator where the DM relic density is proportional to $\frac{m_N T_R^3}{M_{Z'}^4}$ (Eqn.4.14).

In Fig. 9, we numerically solve the Boltzmann equation with the initial condition $Y(x_i) = 0$ for $x_i = 10^{-9}$ and obtain the DM yield as a function of m_N/T for the case $M_{Z'} \ll m_N$. Here we have chosen $m_N = 1\text{TeV}$, $M_{Z'} = 0.1\text{GeV}$, $x_h = -1.2$, $x_\phi = 1$ and $g' = 3.65 \times 10^{-6}$. The resultant $Y_\infty = 4.36 \times 10^{-13}$ reproduces the observed relic density of DM in the universe. The freeze-in occurs at $T \sim 2m_N$. We can obtain similar plots for different choices of x_h and x_ϕ by properly tuning g' to get the correct relic density. For example, with the choice of $x_h = 1$ and $x_\phi = 10$, the coupling should be $g' = 3.15 \times 10^{-7}$ for $\Omega_N h^2 \simeq 0.12$.

In Fig. 10, we have shown the variation of the DM relic density in the $x_h - x_\phi$ plane for $g' = 3.04 \times 10^{-6}$. As in the previous case, here also the DM relic density is more sensitive to the value of the x_ϕ than the x_h value. This can also be seen clearly from Eqn. 4.21. Note that one can take even smaller values of the g' coupling and still get the correct DM relic

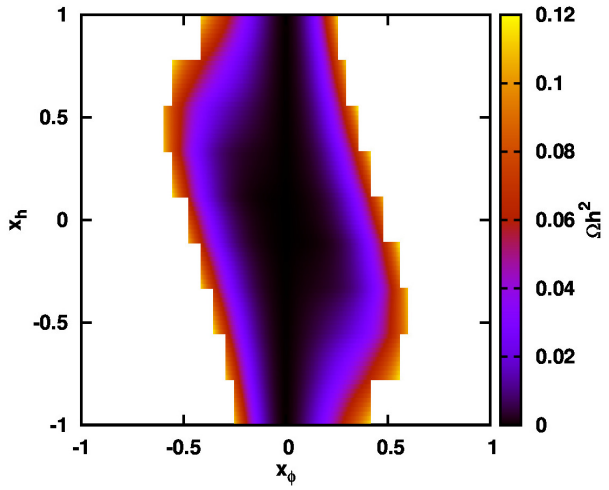

FIG. 10: Relic density plot in $x_h - x_\phi$ plane for case-B discussed in the text. We have fixed $g' = 3.04 \times 10^{-6}$.

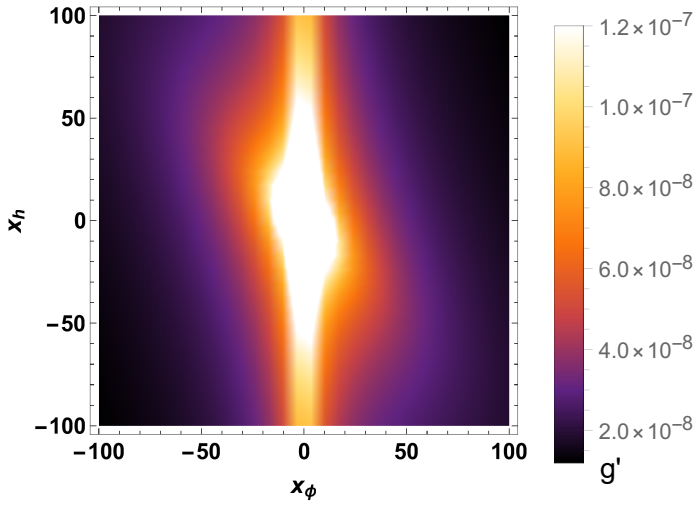

FIG. 11: Variation of the $U(1)'$ gauge coupling with x_h and x_ϕ corresponding to the points that give the correct relic density for sterile neutrino DM in case-B.

density by taking larger values of $|x_h|$ and $|x_\phi|$.

In Fig. 11, we obtain the variation of g' with x_h and x_ϕ corresponding to the parameter space that gives the correct relic density. In general, the value of the gauge coupling decreases with increase in the values of $|x_\phi|$. For $x_h = 0$ and $x_\phi = 1$, the $U(1)'$ model reduces to $U(1)_{B-L}$ model. For this case, to get the correct relic density of sterile neutrino DM

($\Omega_N h^2 \simeq 0.12$), we obtain the gauge coupling from Eqn. 4.21 as $g_{B-L} = 1.6 \times 10^{-6}$. For the points that give the correct relic abundance, the $U(1)'$ coupling and $U(1)_{B-L}$ gauge coupling are related by,

$$g' = 1.89 \times g_{B-L} x_\phi^{-\frac{1}{2}} (10x_h^2 + 13x_\phi^2 + 16x_h x_\phi)^{-\frac{1}{4}}. \tag{4.22}$$

C. DM production from Z' resonance ($m_N \ll M_{Z'} \ll T_R$)

Now we consider the case where the DM is lighter than Z'. In this case, the sterile neutrino DM can be produced through Z' boson resonance [46]. The resonance occurs at $s = M_{Z'}^2$ for $\sqrt{s} \geq 2m_N$. Note that the integration over $\sqrt{s}$ is done from $\sqrt{s} = 2m_N$ to $\sqrt{s} = T_R$, the range in which DM production occurs. The resonant production of DM is not possible in Cases A and B, where $M_Z' \gg T_R \gg m_N$ (and hence $\sqrt{s} << M_{Z'}$) and $M_Z' \ll m_N \ll T_R$ (so that $\sqrt{s} >> M_{Z'}$), respectively. Using the Breit-Wigner formula for narrow width approximation, the Z' propagator can be written as,

$$\frac{1}{(s - M_{Z'}^2)^2 + M_{Z'}^2 \Gamma_{Z'}^2} = \frac{\pi}{M_{Z'}\Gamma_{Z'}} \delta(s - M_{Z'}^2). \tag{4.23}$$

Hence, the cross section for the resonance production of DM for higgh T_R becomes,

$$\sigma(s) = \frac{g'^4}{48\pi} \pi \frac{s\Big(1 - \frac{4m_N^2}{s}\Big)^{\frac{3}{2}}}{M_Z' \Gamma_{Z'}} \delta(s - M_{Z'}^2) x_\phi^2 (10x_h^2 + 13x_\phi^2 + 16x_h x_\phi). \tag{4.24}$$

If the mass of the Z' is such that it cannot decay to top quark ($M_{Z'} < 2m_t \sim 346$ GeV), the total decay width of Z' becomes,

$$\Gamma_{Z'} = \frac{1}{24\pi} g'^2 M_Z' [\frac{1}{36}(241x_h^2 + 418x_\phi^2 + 436x_h x_\phi) + x_\phi^2]. \tag{4.25}$$

Using Eqn. 4.18, Eqn. 4.23, Eqn. 4.24, and Eqn. 4.25, we can write the thermal average cross section as,

$$< \sigma v > \simeq \frac{\pi g'^2 x^5 M_{Z'}^3}{64 m_N^5} K_1\Big(\frac{M_{Z'} x}{m_N}\Big) \Big[\frac{x_\phi^2 (10x_h^2 + 13x_\phi^2 + 16x_h x_\phi)}{\frac{1}{36}(241x_h^2 + 418x_\phi^2 + 436x_h x_\phi) + x_\phi^2}\Big] \Big(1 - \frac{4m_N^2}{M_{Z'}^2}\Big)^{5/2}, \tag{4.26}$$

where $x = m_N/T$. Hence, for $x \lesssim \frac{m_N}{M_{Z'}}$, Eqn. 4.26 becomes,

$$< \sigma v > \simeq \frac{\pi}{64} g'^2 \frac{M_{Z'}^2}{m_N^4} x^4 \Big[\frac{x_\phi^2 (10x_h^2 + 13x_\phi^2 + 16x_h x_\phi)}{\frac{1}{36}(241x_h^2 + 418x_\phi^2 + 436x_h x_\phi) + x_\phi^2}\Big] \Big(1 - \frac{4m_N^2}{M_{Z'}^2}\Big)^{5/2}, \tag{4.27}$$

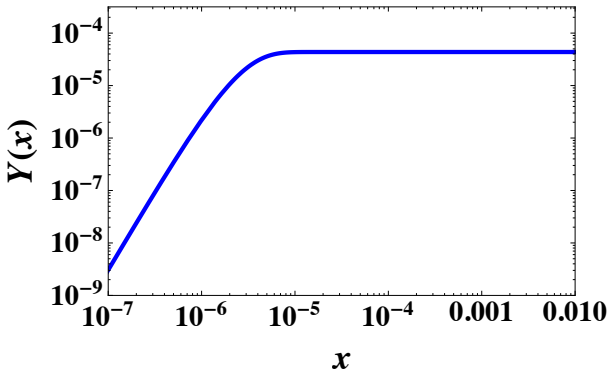

FIG. 12: Variation of the DM yield as a function of $x = \frac{m_N}{T}$ for case-C. We have fixed $M_{Z'} = 10\text{GeV}$, $m_N = 10\text{keV}$, $g' = 2 \times 10^{-9}$ and $x_\phi = 1$, $x_h = -1.2$ in plotting this figure.

where we have used the approximation $K_1\Big(\frac{M_{Z'}x}{m_N}\Big) \sim \frac{m_N}{M_{Z'}x}$ for $x \lesssim \frac{m_N}{M_{Z'}}$. For $x \gtrsim \frac{m_N}{M_{Z'}}$, the first order modified Bessel function is exponentially suppressed and hence, $< \sigma v > \sim 0$. This is because in this limit, $T < M_{Z'}$ and the energy of the SM particles are not enough to produce Z' resonance and hence DM creation rate drops. Now integrating the Boltzmann equation from $x = x_i$ to $x = \frac{m_N}{M_{Z'}}$ and putting the initial condition $Y(x_i) = 0$, we obtain the comoving DM density as,

$$Y_\infty \simeq 4.2 \times 10^{-6} g'^2 \Big(\frac{M_{pl}}{M_{Z'}}\Big)\Big[\frac{x_\phi^2(10x_h^2 + 13x_\phi^2 + 16x_h x_\phi)}{\frac{1}{36}(241x_h^2 + 418x_\phi^2 + 436x_h x_\phi) + x_\phi^2}\Big]\Big(1 - \frac{4m_N^2}{M_{Z'}^2}\Big)^{5/2}. \quad (4.28)$$

Thus, Y_∞ is inversely proportional to the mass of Z' and depends on x_h and x_ϕ. Hence, the relic density of DM becomes,

$$\Omega_N h^2 \simeq 0.12\Big(\frac{g'}{6.54 \times 10^{-9}}\Big)^2\Big(\frac{m_N}{10\text{keV}}\Big)\Big(\frac{10\text{GeV}}{M_{Z'}}\Big)\Big[\frac{x_\phi^2(10x_h^2 + 13x_\phi^2 + 16x_h x_\phi)}{\frac{1}{36}(241x_h^2 + 418x_\phi^2 + 436x_h x_\phi) + x_\phi^2}\Big]\Big(1-\frac{4m_N^2}{M_{Z'}^2}\Big)^{5/2}. \quad (4.29)$$

On the other hand, if Z' can decay to top quark, then the relic density of the DM in $T_R \gg M'_Z \gg m_N$ limit is modified as,

$$\Omega_N h^2 \simeq 0.12\Big(\frac{g'}{6.54 \times 10^{-9}}\Big)^2\Big(\frac{m_N}{10\text{keV}}\Big)\Big(\frac{10\text{GeV}}{M_{Z'}}\Big)\Big[\frac{x_\phi^2(10x_h^2 + 13x_\phi^2 + 16x_h x_\phi)}{(10x_h^2 + 13x_\phi^2 + 16x_h x_\phi) + x_\phi^2}\Big]\Big(1-\frac{4m_N^2}{M_{Z'}^2}\Big)^{\frac{5}{2}}. \quad (4.30)$$

Thus, the DM relic density increases with m_N and decreases with $M_{Z'}$.

We obtain the DM yield as a function of m_N/T in Fig. 12 for case-C ($m_N \ll M_{Z'} \ll T_R$) by numerically solving the Boltzmann equation with the initial condition $Y(x_i) = 0$, where

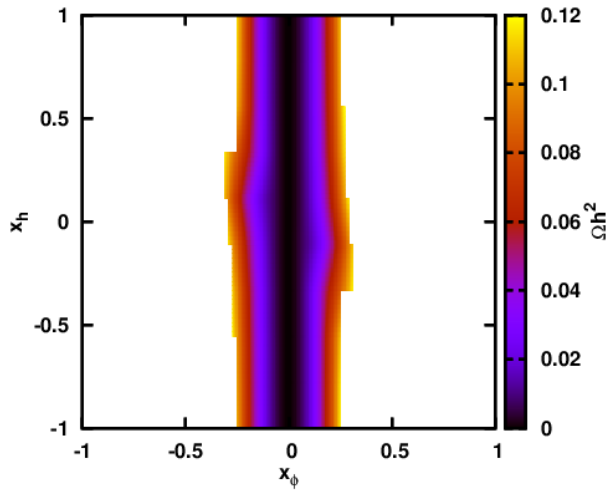

FIG. 13: Relic density plot in $x_h - x_\phi$ plane for case-C. We have fixed $g' = 6.54 \times 10^{-9}, m_N = 10\text{keV}$ and $M_{Z'} = 1\text{GeV}$.

$x_i = 10^{-9}$. We have fixed $M_{Z'} = 10\text{GeV}$, $m_N = 10\text{keV}$, $g' = 2 \times 10^{-9}$ and $x_\phi = 1$, $x_h = -1.2$ in plotting this figure. The resultant $Y_\infty = 4.36 \times 10^{-5}$ gives the correct relic density. Note that here, the freeze-in occurs at $x = m_N/M_{Z'}$ (i.e., at $T = M_{Z'}$). As in the previous cases, we can obtain similar plots for different values of x_h and x_ϕ by properly tuning g' to reproduce the correct relic density. For instance, if we fix $x_h = 1$ and $x_\phi = 10$, the correct relic density can be obtained by choosing $g' = 1.42 \times 10^{-10}$.

In Fig. 13, we have shown the variation of the DM relic density in the $x_h - x_\phi$ plane. We have fixed $g' = 6.54 \times 10^{-9}, m_N = 10\text{keV}$ and $M_{Z'} = 1\text{GeV}$. As in the previous cases, here also the relic density is more sensitive to x_ϕ than x_h and we can take even smaller values of $U(1)'$ gauge coupling and get the correct relic density by taking very large values of x_h and x_ϕ. Also note that such large values of x_h and x_ϕ do not violate perturbativity since the bounds are on the products of g' with x_h and x_ϕ as can be seen from Eqn. 3.6.

In Fig. 14, we have shown the variation of the gauge coupling in the $x_h - x_\phi$ plane corresponding to the points which give the correct relic density. In plotting this, we have fixed the parameters $m_N = 10\text{keV}$ and $M_{Z'} = 1\text{GeV}$. Again, one can see that the value of g' that gives the correct relic density decreases with increase in the value of x_ϕ.

In Fig. 15, we have shown the variation of the DM relic density with the mass of the DM

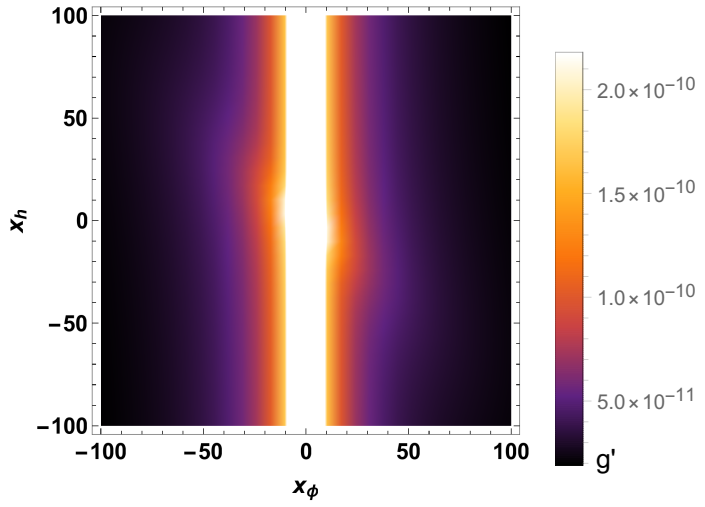

FIG. 14: Variation of the $U(1)'$ gauge coupling in $x_h - x_\phi$ plane corresponding to the points that give the correct relic density for case-C. Here, we have fixed the parameters $m_N = 10\text{keV}$ and $M_{Z'} = 1\text{GeV}$.

and the $U(1)'$ gauge boson. In the upper panel, we have shown the variation of relic density with respect to the DM mass for different values of M'_Z, g', x_h and x_ϕ. In the lower panel, we have shown the variation of DM relic density with M'_Z for different values of DM masses, gauge coupling, x_h and x_ϕ. The relic density of the DM increases with increase in the DM mass and it decreases with the $U(1)'$ gauge boson mass as expected from Eqn. 4.29. The cut-off in these plots is dictated by the factor $\left(1 - \frac{4m_N^2}{M_{Z'}^2}\right)$ in Eqn. 4.30, which demands that $M_{Z'} \geq 2m_N$.

In Fig. 16, we have shown the variation of the gauge coupling with DM mass corresponding to the points which give the correct relic density for different values of $M_{Z'}$. We have chosen $x_h = 1, x_\phi = 1$ for the left panel and $x_h = 5, x_\phi = 5$ for the right panel. The required value of the gauge coupling to give the correct relic density decreases with increase in the DM mass and with decrease in the gauge boson mass. Here also, the cut-off in m_N is due to the above mentioned requirement $M_{Z'} \geq 2m_N$.

Now let us consider the case of the $U(1)_{B-L}$ model taking $x_h = 0$ and $x_\phi = 1$. To get the correct relic density $\Omega_N h^2 \simeq 0.12$, the $U(1)'$ gauge coupling has to be $g_{B-L} = 1.00 \times 10^{-11}\sqrt{\frac{m'_Z}{m_N}}$. For $M_{Z'} = 10\text{GeV}$ and $m_N = 10\text{keV}$, the $B - L$ coupling becomes

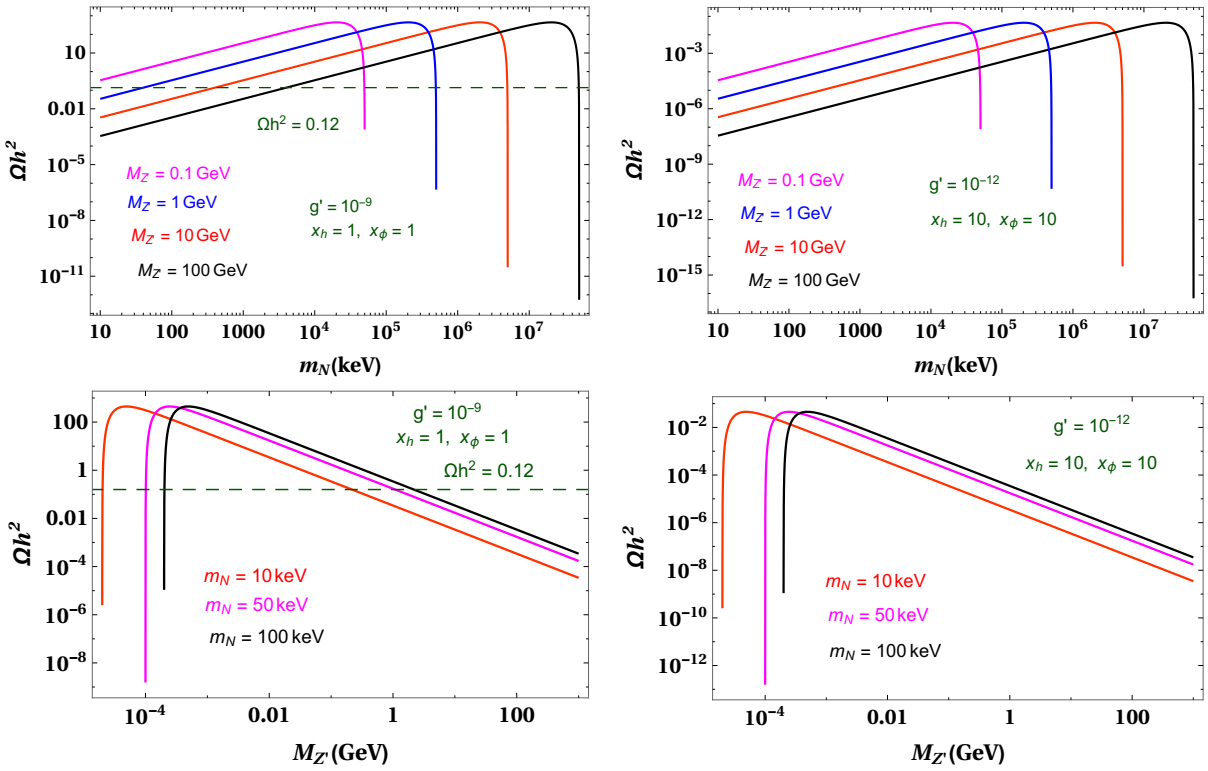

FIG. 15: Variation of relic density with the masses of the DM and the $U(1)'$ gauge boson for case-C. In the upper panels, we have shown the variation of relic density with respect to the DM mass for different M'_Z, g' and x_h, x_ϕ. In the lower panels, we have shown the variation of relic DM density with M'_Z for different DM mass, g' and x_h, x_ϕ.

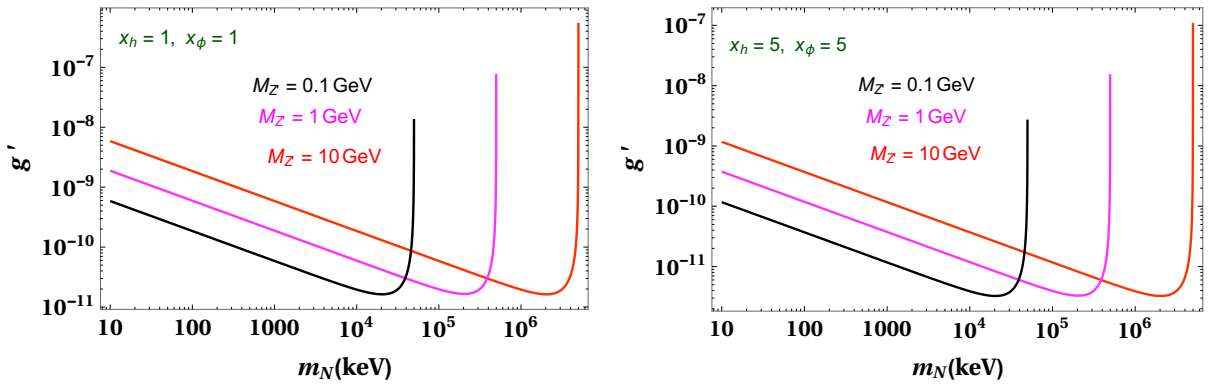

FIG. 16: Variation of the gauge coupling with DM mass for different Z' mass corresponding to the points that give the correct relic density in case-C. We have chosen $x_h = 1, x_\phi = 1$ (left panel) and $x_h = 5, x_\phi = 5$ (right panel).

$g_{B-L} = 1.00 \times 10^{-8}$. The $U(1)'$ coupling and $U(1)_{B-L}$ coupling are related by the expression,

$$g' = 1.01 \times g_{B-L} \Big[\frac{x_\phi^2 (10 x_h^2 + 13 x_\phi^2 + 16 x_h x_\phi)}{\frac{1}{36}(241 x_h^2 + 418 x_\phi^2 + 436 x_h x_\phi) + x_\phi^2} \Big]^{-\frac{1}{2}}. \tag{4.31}$$

For $U(1)'$ gauge boson mass much greater than the sterile neutrino DM ($M_{Z'} \gg m_N$), using $M_{Z'} \sim x_\phi g' u$, we can get an expression for the vev of Φ, u as,

$$u \sim 4.82 \times 10^8 \text{GeV} \sqrt{\frac{M'_Z}{1\text{GeV}}} \sqrt{\frac{m_N}{10\text{keV}}} \Big[\frac{(10 x_h^2 + 13 x_\phi^2 + 16 x_h x_\phi)}{\frac{1}{36}(241 x_h^2 + 418 x_\phi^2 + 436 x_h x_\phi) + x_\phi^2} \Big]^{\frac{1}{2}} \Big(1 - \frac{4 m_N^2}{M'_Z} \Big)^{\frac{5}{4}}. \tag{4.32}$$

V. BOUNDS ON Z' MASS FROM EXPERIMENTS

The Z' in this $U(1)'$ model can also be searched for in various experiments. In particular, a heavy Z' boson ($M_{Z'} \sim \mathcal{O}$ (TeV)) can be searched in the ATLAS experiment whereas a light Z' ($M_{Z'} \sim 10^{-4} - 100$ GeV) can be observed in the future lifetime frontier experiments such as SHiP [51] and FASERs [52, 53]. For the former case, we discuss the existing bounds from the ATLAS experiment for different choices of x_h and x_ϕ. For the DM scenarios with a light Z', we compare the parameter space allowed by the DM relic density with the existing astrophysical constraints as well as with the parameter space that can be probed in the future lifetime frontier experiments, for the special case of $U(1)_{B-L}$ model ($x_h = 0, x_\phi = 1$).

A. Heavy Z'

In this section, we study the bounds on the mass of the heavy Z' gauge boson and the coupling strength g' from the collider experiments. Particularly, we study the bounds in the $M_{Z'} - g'$ planes for different values of x_h and x_ϕ and compare it with the parameter space that gives the correct DM relic density, $\Omega_N h^2 \simeq 0.12$. First we consider case-A discussed in section - IV.

In Figs. 17 and 18, we have shown the variation of g' with $M_{Z'}$ for different values of x_h, x_ϕ, T_R and m_N. The solid red, dashed red, solid black and dashed black lines correspond to the lines that give the correct relic density $\Omega_N h^2 \simeq 0.12$ for $(T_R, m_N) = (20$ MeV, 1 MeV),

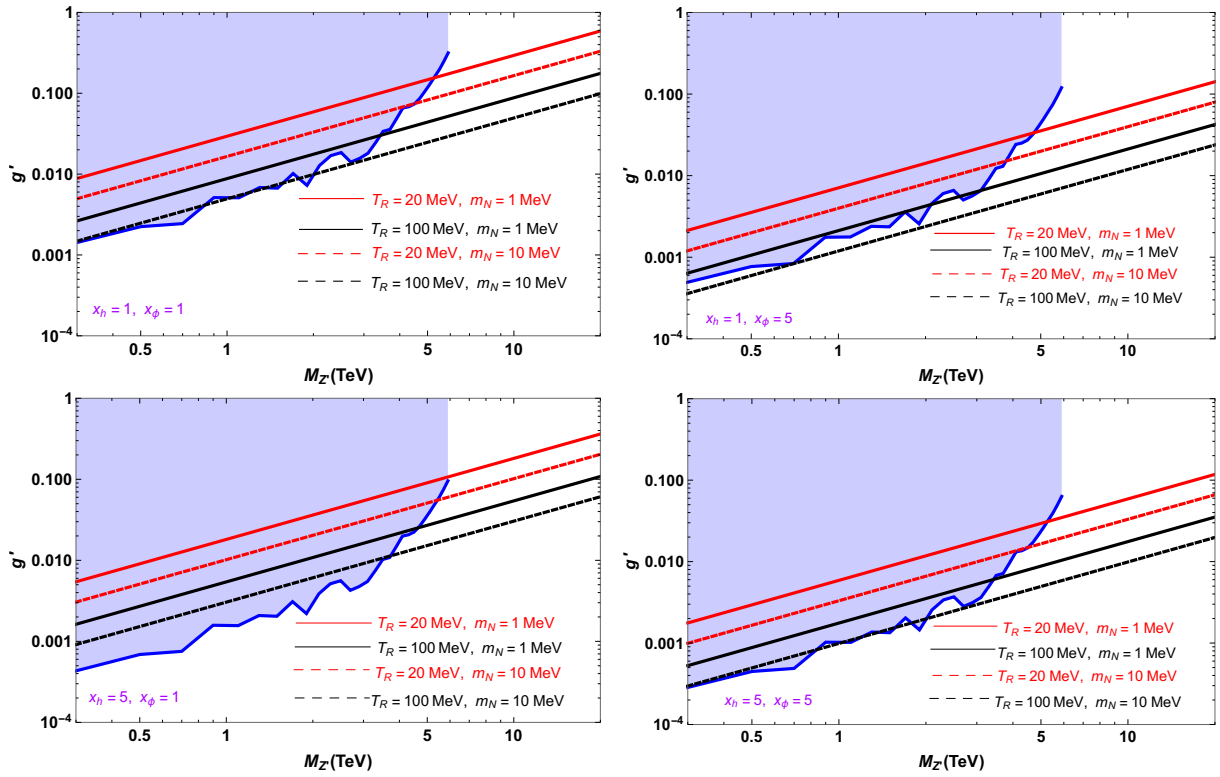

FIG. 17: Variation of g' with $M_{Z'}$ for different values of x_h, x_ϕ, T_R and m_N. The solid red, dashed red, solid black and dashed black lines correspond to the lines that give the correct relic density $\Omega_N h^2 \simeq 0.12$ for (T_R, m_N) = (20 MeV, 1 MeV), (20 MeV, 10 MeV), (100 MeV, 1 MeV) and (100 MeV, 10 MeV) respectively. The blue shaded regions are disfavored by the ATLAS search for a heavy Z' [103].

(20 MeV, 10 MeV), (100 MeV, 1 MeV) and (100 MeV, 10 MeV) respectively. The blue shaded regions are disfavored by the ATLAS search for a heavy Z' [20, 103]. The ATLAS has given bounds on the cross section for the process $pp \to Z' \to 2e, 2\mu$ for the sequential Standard Model (SSM). We have used this to obtain the bounds in the $M_{Z'} - g'$ planes for other models with different values of x_h and x_ϕ. The bound on the g' value corresponding to a given $M_{Z'}$ value is then obtained as,

$$g' = \sqrt{\frac{\sigma^{\rm Observed}_{\rm ATLAS}}{\left(\frac{\sigma_{\rm Model}}{g'^{\,2}_{Model}}\right)}}, \tag{5.1}$$

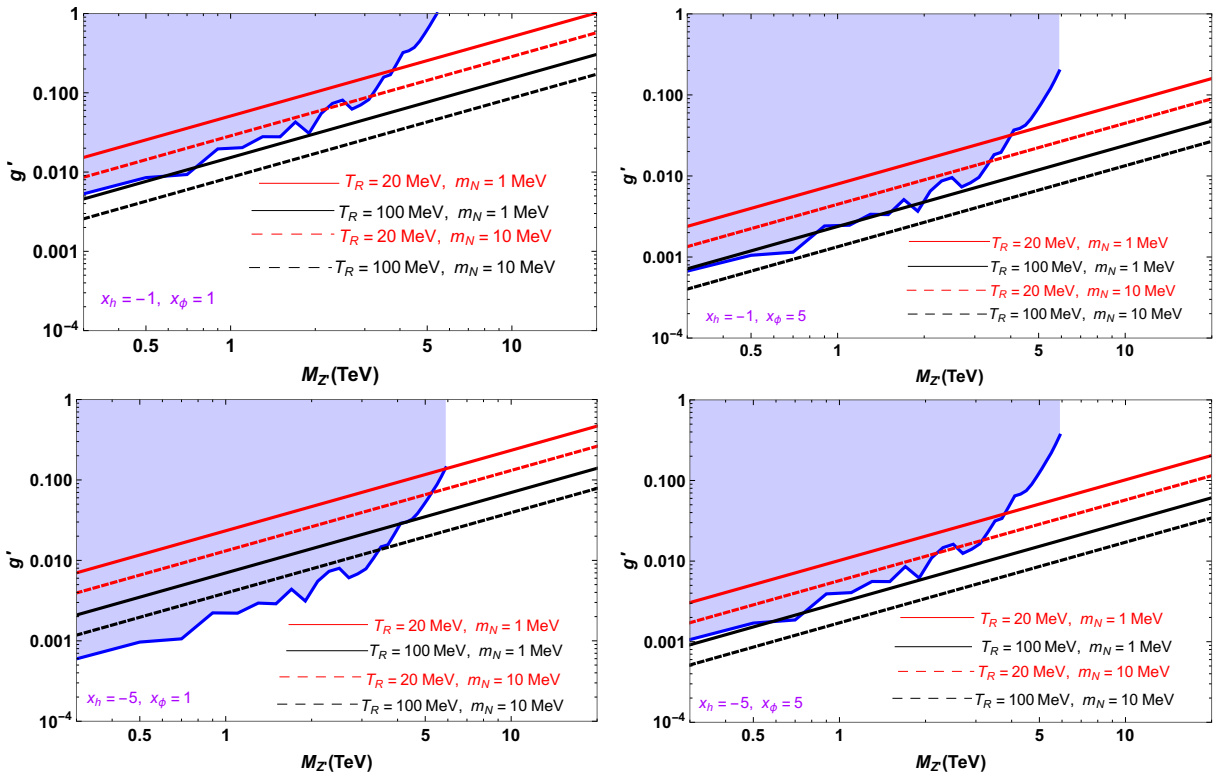

FIG. 18: Same as Fig. 17, but for different values of x_h and x_ϕ.

where $\sigma^{\text{Observed}}_{\text{ATLAS}}$ is the observed bound from ATLAS and σ_{Model} is the calculated value of the cross section for the given model. In Figs. 17 and 18, the parts of the lines that are in the white region correspond to the points of the parameter space that give the correct relic density for a given T_R and m_N. These regions can be probed in the future runs of the collider experiments. One can see that the values of the allowed coupling strength increases with increasing $M_{Z'}$ as already seen previously. Also, it can be seen that the most stringent bound from ATLAS is on the case with $x_h = 5$ and $x_\phi = 5$ whereas the case with $x_h = -1$ and $x_\phi = 1$ has the largest allowed parameter space.

B. Light Z'

To obtain the correct relic density of sterile neutrino DM through light Z' portal, the coupling should be very small and the Z' boson has to be long lived as we have seen in the

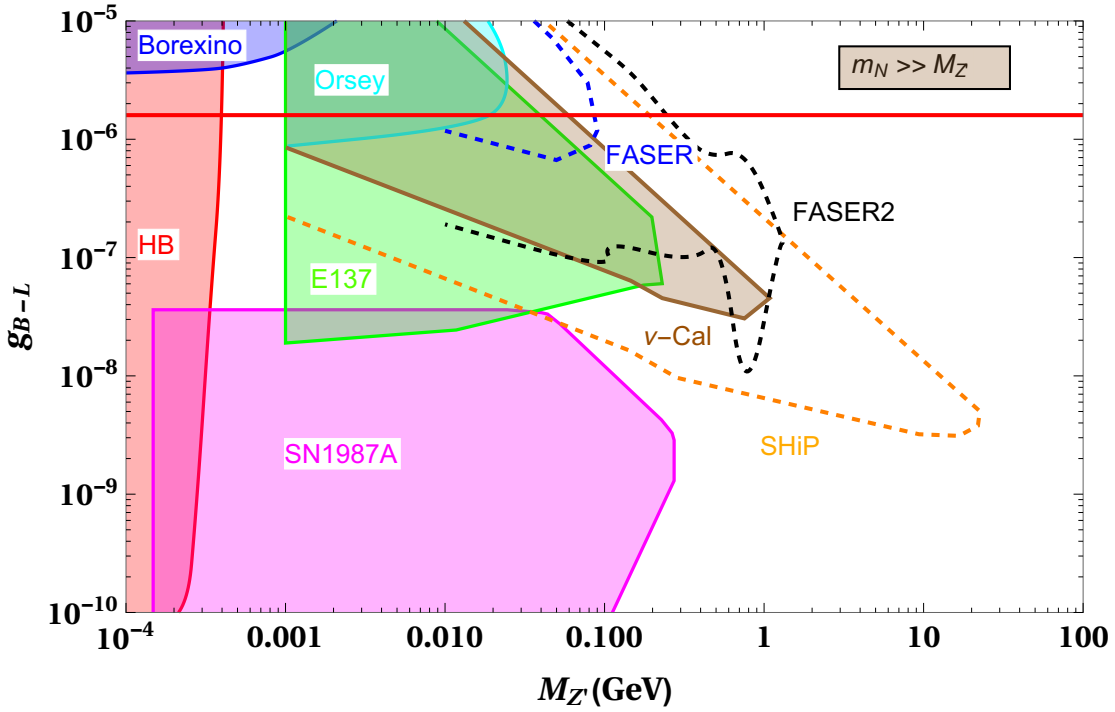

FIG. 19: Constraints in the $M_{Z'} - g'$ plane for the $U(1)_{B-L}$ model. The solid horizontal red line correspond to the points that give the correct relic density of DM in the $g' - M_{Z'}$ plane. Here we have considered the case-B discussed in section-IV where $m_N \gg M_{Z'}$.

previous section. The parameter space for such a light Z' can be probed in several proposed experiments. In Figs. 19 and 20, we have shown the various existing bounds as well as future senstivities of the planned experiments in the $M_{Z'} - g'$ planes for the $U(1)_{B-L}$ case with light Z'.

We have also shown various astrophysical bounds. The rate of energy loss of stars due to the emission of lighter Z' in globular clusters [104, 105] shortens the lifetime of the stars which put bounds on Z' mass and coupling in the $g' - M_{Z'}$ plane as shown by the red shaded regions in Figs. 19 and 20. The supernova 1987A (SN1987A) also puts bound on Z' mass and coupling from energy loss due to the emission of light particles which changes the signal duration of neutrinos [104, 106, 107]. The bounds from SN1987A is shown by the pink shaded regions. The observed neutrino electron scattering experiment by Borexino from 867keV ^7Be solar neutrino [108] agrees well with the SM prediction and hence the ratio of

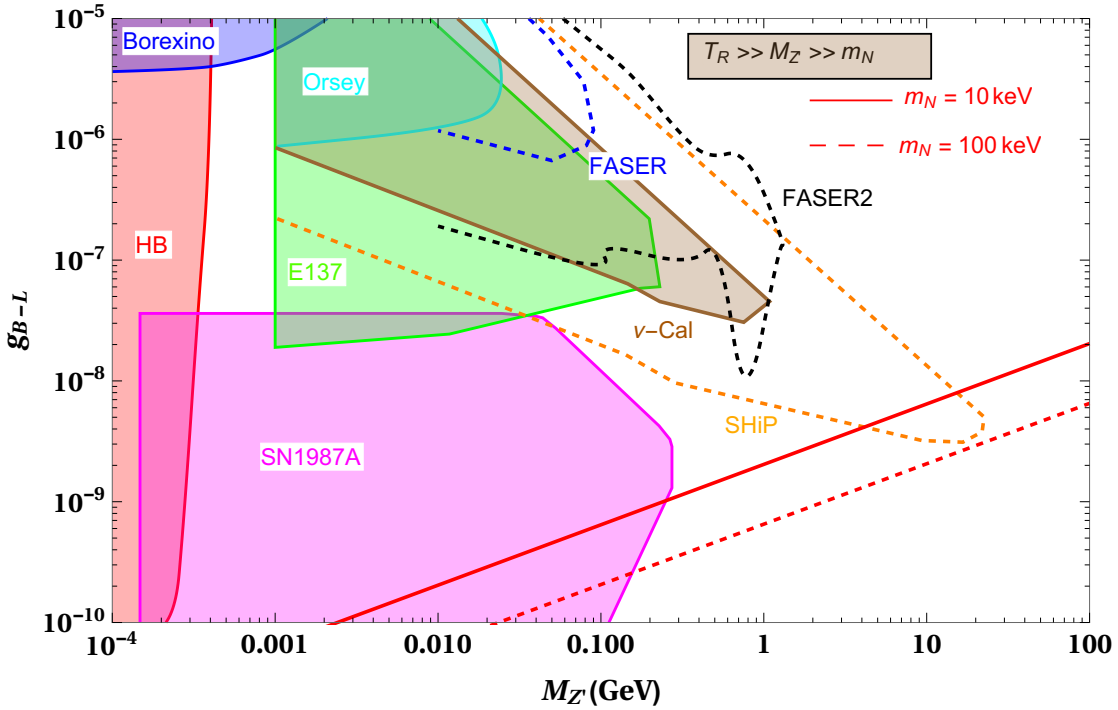

FIG. 20: Constraints in the $M_{Z'} - g'$ plane for the $U(1)_{B-L}$ model. The solid and dashed-slanted red lines in the lower right side give the parameter space that give the correct DM relic density for $m_N = 10$ keV and 100 keV, respectively. Here we considered the case-C discussed in section-IV where $T_R >> M_{Z'} >> m_N$.

the cross sections between Z' involved process and the SM prediction should not exceed the maximum error [109]. This puts bound on Z' mass and coupling and it is shown by dark blue region. The constraints from the various electron proton beam dump experiments are shown by the cyan (Orsey) [110], brown (ν-Cal) [111] and green regions (E137)[112]. The orange dashed curve denotes the expected reach of SHiP based only on the proton bremsstrahlung [51, 113]. It can cover a mass range of 1MeV $\lesssim M'_Z \lesssim$ 200MeV. The proposed FASER and FASER 2 experiments [52, 53, 114] can probe long lived Z' gauge boson in the mass range 10MeV << $M_{Z'}$ << 1GeV. These are shown by the dotted blue and black lines respectively.

The solid horizontal red line in Fig. 19 corresponds to the points that give the correct relic density of DM in the $M_{Z'} - g_{B-L}$ plane. Here we considered the $m_N \gg M_{Z'}$ limit (case-B) and as we had seen earlier in Eqn.4.21, the DM relic density in this case is independent of

the masses of the DM candidate as well as the Z' boson. The region above the red line is disfavored by the overabundance of DM relic density. In the allowed parameter space, some points are already disfavored by the existing constraints whereas a part of the allowed parameter space can be probed by future experiments.

In Fig. 20, we have considered the case-C where $T_R >> M_{Z'} >> m_N$. The slanted red lines in the lower right side give the parameter space that give the correct DM relic density, with the solid and dashed lines corresponding to the mass of the DM candidate m_N =10 keV and 100 keV, respectively. We can see that the value of the gauge coupling increases with increasing $M_{Z'}$ and with decreasing m_N. Here also, the region above the red line is disfavored by the overabundance of the DM relic density. A small part of the allowed parameter space can be probed in the SHiP experiment.

VI. INTEGRAL ANOMALY AND GALACTIC 511 keV LINE

The decay of the $\mathcal{O}$(MeV) sterile neutrino DM in our $U(1)'$ model can account for the galactic 511 keV line observed by the INTEGRAL satellite [54, 55]. The DM particles can annihilate [115–119] or decay [120–127] to produce low energy e^+e^- pairs which could be the origin of the signal. Due to the collision with background baryonic matter, the positrons loose its kinetic energy and form positronium which is an unstable bound system of electron and positron. Thereafter depending on their relative spin states, the positronium annihilates into photons of 511keV line. The DM particles involved in the process are very light, as light as the electron, because otherwise the positrons would be too energetic to produce positronium. The γ ray photon flux observed by the INTEGRAL satellite at 2σ level is [55],

$$\Phi_{511} = (1.05 \pm 0.06) \times 10^{-3} \text{photon/cm}^2\text{/sec.} \tag{6.1}$$

In our model, the charged current Lagrangian can be written as,

$$\mathcal{L}_{cc} = \frac{g}{\sqrt{2}} W_\mu \bar{l} \gamma^\mu P_L (U_{li}\nu_i + V_{lj} N_j) + \text{h.c.}, \tag{6.2}$$

where P_L is the left chiral projection operator and g is the $SU(2)_L$ gauge coupling. We can also write the neutral current Lagrangian as,

$$\mathcal{L}_{NC} = -\Big(\frac{g}{2\cos\theta_w} Z_\mu + g' q_\nu Z'_\mu\Big)\Big[(U^\dagger U)_{ij}\bar{\nu_i}\gamma^\mu P_L \nu_n + (U^\dagger V)_{ij}\bar{\nu_i}\gamma^\mu P_L N_n + (V^\dagger V)_{ij}\bar{N_i}\gamma^\mu P_L N_n\Big] + h.c., \tag{6.3}$$

where θ_w is the Weinberg angle, q_ν is the $U(1)'$ charge of neutrino and g' is the $U(1)'$ gauge coupling. From the above Lagrangian, the off-shell W mediated leptonic partial decay width of the sterile neutrino DM can be calculated as,

$$\Gamma^{W^*}(N_i \to \ell_{L_\alpha}\ell_{L_\beta}\nu_k) = \frac{G_F^2}{192\pi^3} m_{N_i}^5 |V_{\alpha i}|^2 |\mathrm{U_{PMNS\beta k}}|^2. \tag{6.4}$$

Similarly the off-shell Z mediated leptonic partial decay width of the sterile neutrino is given by,

$$\Gamma^{Z^*}(N_i \to \nu_\alpha \ell_{R_\beta}\ell_{R_k}) = \frac{G_F^2}{192\pi^3} m_{N_i}^5 |V_{\alpha i}|^2 \delta_{\beta k} \sin^4\theta_w, \tag{6.5}$$

for the right handed fermions and,

$$\Gamma^{Z^*}(N_i \to \nu_\alpha \ell_{L_\beta}\ell_{L_k}) = \frac{G_F^2}{192\pi^3} m_{N_i}^5 |V_{\alpha i}|^2 \delta_{\beta k} \frac{\cos^2 2\theta_w}{4}, \tag{6.6}$$

for the left handed fermions, respectively. The interference between the off-shell W and off-shell Z mediated modes can be written as,

$$\Gamma^{Z^*/W^*}(N_i \to \nu_\alpha l_\alpha l_\alpha) = \frac{G_F^2}{96\pi^3} m_{N_i}^5 |V_{\alpha i}|^2 \mathrm{Re}[\mathrm{U_{PMNS_{ii}}}]. \tag{6.7}$$

In our analysis we consider the leptons to be the electrons, positrons as the charged leptons. In these expressions θ_w denotes the weak mixing angle. Adding all the contribution, we obtain the total decay width relevant for our analysis as,

$$\Gamma(N \to \nu e^+ e^-) = 5.278 \times \frac{G_F^2}{192\pi^3} m_{N_i}^5 |V_{\alpha i}|^2. \tag{6.8}$$

We consider $m_e \ll m_N$ in calculating the decay width. Here the Z' contribution is not taken into account because its effect is smaller than others. G_F is the Fermi constant and $V_{\alpha i}$ includes the mixing angle. The 511 keV gamma ray flux from the decaying DM can be written as [120, 121],

$$\Phi_{511} \sim 10^{-3}\Big(\frac{10^{27}\,\mathrm{sec}}{\Gamma(N \to \nu e^+ e^-)^{-1}}\Big)\Big(\frac{1\ \mathrm{MeV}}{m_N}\Big)\mathrm{photon/cm^2/sec}. \tag{6.9}$$

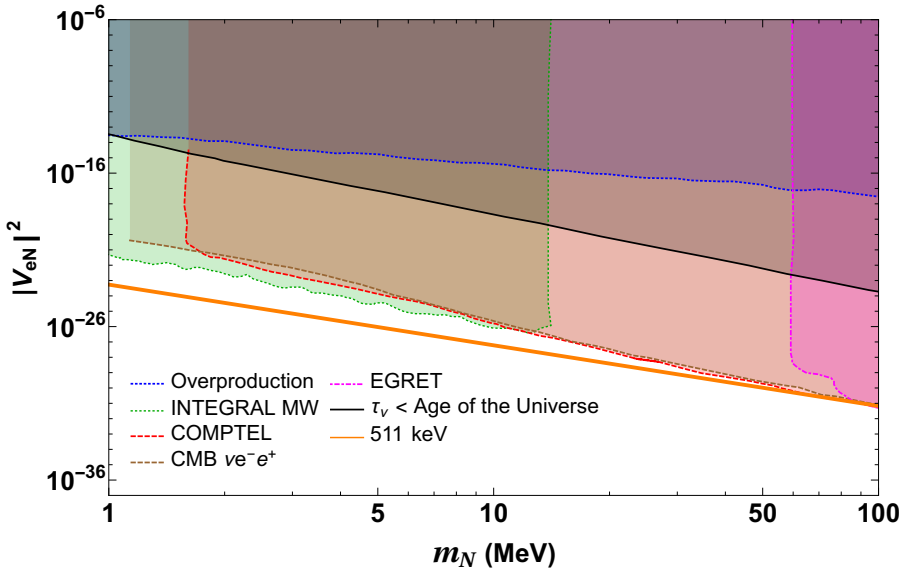

FIG. 21: The orange line corresponds to the values of the masses and mixing of the sterile neutrino DM that can produce the 511 keV line. We have also displayed the existing experimental bounds that were discussed in FIG. 1.

From Eqn. 6.8 and Eqn. 6.9 we can find out the mixing angle for which the decaying DM can give rise to 511 keV excess and

$$|V_{\alpha i}|^2 \Big(\frac{m_N}{1\ \text{MeV}}\Big)^4 \simeq 5.44 \times 10^{-24}. \tag{6.10}$$

For 1 MeV DM the corresponding mixing angle is $|V_{\alpha i}|^2 \sim 5.44 \times 10^{-24}$.

In Fig. 21, the orange line corresponds to the values of the masses and mixing of the sterile neutrino DM that can produce the 511 keV line. We have also displayed the existing experimental constraints that were discussed in FIG. 1. As can be seen from this figure, for 1 MeV $\leq m_N \leq$ 70 MeV, the values of the active-sterile mixing needed to produce the 511 keV line are consistent with all the existing bounds.

VII. CONCLUSIONS

We have studied a class of general U(1)$'$ models to explain the observed dark matter (DM) relic abundance and light neutrino masses. In addition to the SM fermions, the model

contains three right handed neutrinos and three gauge singlet Majorana fermions and the light neutrino mass is generated via the inverse seesaw mechanism, with the heavy neutrino sector consisting of three pairs of pseudo-Dirac neutrinos. One pair of the degenerate sterile neutrinos has been assigned to be the DM candidate whose relic density is generated by the freeze-in mechanism. We have considered the scenario in which the DM particles are produced by the scattering of the SM particles, mediated by the Z' gauge boson. Different regimes of the masses of the DM particle and the Z' gauge boson have been considered. The production of the DM can occur at different reheating temperatures in various scenarios depending on the masses of the Z' boson and the DM particle. We have observed that the the model parameters, especially the $U(1)'$ gauge coupling (g'), the mass of the Z' gauge boson ($M_{Z'}$) and the $U(1)'$ charges of the two scalars in the model (x_h and x_ϕ), receive constraints from the requirements of satisfying the DM relic abundance, vacuum stability and perturbativity. We have also studied the impact of the bounds from the collider searches of heavy Z' at the LHC in the case where $M_{Z'} \sim \mathcal{O}(\text{TeV})$ on the model parameter space. For the cases with a light Z' ($M_{Z'} \sim 10^{-4} - 100$ GeV), we have compared the parameter space allowed by the DM relic density with the bounds from various astrophysical observations as well as with the parameter space that can be tested at the future lifetime frontier experiments SHiP and FASERs, for the special case of $U(1)_{B-L}$ model. We also noted that if the mass of the sterile neutrino DM is $\gtrsim$ 1MeV and if Z' is heavy, the decay of the DM particle into positrons can explain the long standing puzzle of galactic 511keV line in the Milky Way center observed by the INTEGRAL satellite.

ACKNOWLEDGEMENTS

The work of A. D. is supported by the National Research Foundation of Korea (NRF) grant funded by the Korean government (NRF-2020R1C1C1012452).

---

[1] **CMS** Collaboration, S. Chatrchyan *et al.*, "Observation of a New Boson at a Mass of 125 GeV with the CMS Experiment at the LHC," *Phys. Lett. B* **716** (2012) 30–61,

arXiv:1207.7235 [hep-ex].

[2] **ATLAS** Collaboration, G. Aad *et al.*, "Observation of a new particle in the search for the Standard Model Higgs boson with the ATLAS detector at the LHC," *Phys. Lett. B* **716** (2012) 1–29, arXiv:1207.7214 [hep-ex].

[3] **Particle Data Group** Collaboration, P. Zyla *et al.*, "Review of Particle Physics," *PTEP* **2020** no. 8, (2020) 083C01.

[4] **Planck** Collaboration, P. Ade *et al.*, "Planck 2015 results. XIII. Cosmological parameters," *Astron. Astrophys.* **594** (2016) A13, arXiv:1502.01589 [astro-ph.CO].

[5] J. L. Hewett and T. G. Rizzo, "Low-Energy Phenomenology of Superstring Inspired E(6) Models," *Phys. Rept.* **183** (1989) 193.

[6] A. Leike, "The Phenomenology of extra neutral gauge bosons," *Phys. Rept.* **317** (1999) 143–250, arXiv:hep-ph/9805494 [hep-ph].

[7] P. Langacker, "The Physics of Heavy Z' Gauge Bosons," *Rev. Mod. Phys.* **81** (2009) 1199–1228, arXiv:0801.1345 [hep-ph].

[8] P. Minkowski, "$\mu \to e\gamma$ at a Rate of One Out of 10^9 Muon Decays?," *Phys. Lett.* **67B** (1977) 421–428.

[9] R. N. Mohapatra and G. Senjanovic, "Neutrino Mass and Spontaneous Parity Nonconservation," *Phys. Rev. Lett.* **44** (1980) 912.

[10] S. M. Boucenna, S. Morisi, and J. W. Valle, "The low-scale approach to neutrino masses," *Adv. High Energy Phys.* **2014** (2014) 831598, arXiv:1404.3751 [hep-ph].

[11] R. Mohapatra and J. Valle, "Neutrino Mass and Baryon Number Nonconservation in Superstring Models," *Phys. Rev. D* **34** (1986) 1642.

[12] S. Khalil and O. Seto, "Sterile neutrino dark matter in B - L extension of the standard model and galactic 511-keV line," *JCAP* **10** (2008) 024, arXiv:0804.0336 [hep-ph].

[13] N. Okada and O. Seto, "Higgs portal dark matter in the minimal gauged $U(1)_{B-L}$ model," *Phys. Rev. D* **82** (2010) 023507, arXiv:1002.2525 [hep-ph].

[14] S. Oda, N. Okada, and D.-s. Takahashi, "Right-handed neutrino dark matter in the classically conformal U(1)' extended standard model," *Phys. Rev. D* **96** no. 9, (2017) 095032, arXiv:1704.05023 [hep-ph].

[15] P. Bandyopadhyay, E. J. Chun, and R. Mandal, "Implications of right-handed neutrinos in $B - L$ extended standard model with scalar dark matter," *Phys. Rev. D* **97** no. 1, (2018) 015001, arXiv:1707.00874 [hep-ph].

[16] S. Singirala, R. Mohanta, and S. Patra, "Singlet scalar Dark matter in $U(1)_{B-L}$ models without right-handed neutrinos," *Eur. Phys. J. Plus* **133** no. 11, (2018) 477, arXiv:1704.01107 [hep-ph].

[17] S. Singirala, R. Mohanta, S. Patra, and S. Rao, "Majorana Dark Matter in a new BL model," *JCAP* **11** (2018) 026, arXiv:1710.05775 [hep-ph].

[18] A. Biswas, S. Choubey, and S. Khan, "Neutrino mass, leptogenesis and FIMP dark matter in a $\mathrm{U}(1)_{B-L}$ model," *Eur. Phys. J. C* **77** no. 12, (2017) 875, arXiv:1704.00819 [hep-ph].

[19] N. Okada, S. Okada, and D. Raut, "Natural Z' -portal Majorana dark matter in alternative U(1) extended standard model," *Phys. Rev. D* **100** no. 3, (2019) 035022, arXiv:1811.11927 [hep-ph].

[20] A. Das, S. Goswami, K. Vishnudath, and T. Nomura, "Constraining a general $\mathrm{U}(1)'$ inverse seesaw model from vacuum stability, dark matter and collider," *Phys. Rev. D* **101** no. 5, (2020) 055026, arXiv:1905.00201 [hep-ph].

[21] W. Abdallah, S. Choubey, and S. Khan, "FIMP dark matter candidate(s) in a BL model with inverse seesaw mechanism," *JHEP* **06** (2019) 095, arXiv:1904.10015 [hep-ph].

[22] P. Bandyopadhyay, M. Mitra, and A. Roy, "Relativistic Freeze-in with Scalar Dark Matter in a Gauged $B - L$ Model and Electroweak Symmetry Breaking," arXiv:2012.07142 [hep-ph].

[23] **XENON** Collaboration, E. Aprile *et al.*, "Dark Matter Search Results from a One Ton-Year Exposure of XENON1T," *Phys. Rev. Lett.* **121** no. 11, (2018) 111302, arXiv:1805.12562 [astro-ph.CO].

[24] **LUX** Collaboration, D. Akerib *et al.*, "First results from the LUX dark matter experiment at the Sanford Underground Research Facility," *Phys. Rev. Lett.* **112** (2014) 091303, arXiv:1310.8214 [astro-ph.CO].

[25] **PandaX-II** Collaboration, X. Cui *et al.*, "Dark Matter Results From 54-Ton-Day Exposure of PandaX-II Experiment," *Phys. Rev. Lett.* **119** no. 18, (2017) 181302, arXiv:1708.06917

[astro-ph.CO].

[26] L. J. Hall, K. Jedamzik, J. March-Russell, and S. M. West, "Freeze-In Production of FIMP Dark Matter," *JHEP* **03** (2010) 080, arXiv:0911.1120 [hep-ph].

[27] Y. Hochberg, E. Kuflik, T. Volansky, and J. G. Wacker, "Mechanism for Thermal Relic Dark Matter of Strongly Interacting Massive Particles," *Phys. Rev. Lett.* **113** (2014) 171301, arXiv:1402.5143 [hep-ph].

[28] T. Kumar Poddar, S. Mohanty, and S. Jana, "Vector gauge boson radiation from compact binary systems in a gauged $L_\mu - L_\tau$ scenario," *Phys. Rev. D* **100** no. 12, (2019) 123023, arXiv:1908.09732 [hep-ph].

[29] T. Kumar Poddar, S. Mohanty, and S. Jana, "Constraints on long range force from perihelion precession of planets in a gauged $L_e - L_{\mu,\tau}$ scenario," arXiv:2002.02935 [hep-ph].

[30] G. Choi, T. T. Yanagida, and N. Yokozaki, "Feebly Interacting $U(1)_{\rm B-L}$ Gauge Boson Warm Dark Matter and XENON1T Anomaly," arXiv:2007.04278 [hep-ph].

[31] W. Hu, R. Barkana, and A. Gruzinov, "Cold and fuzzy dark matter," *Phys. Rev. Lett.* **85** (2000) 1158–1161, arXiv:astro-ph/0003365.

[32] L. D. Duffy and K. van Bibber, "Axions as Dark Matter Particles," *New J. Phys.* **11** (2009) 105008, arXiv:0904.3346 [hep-ph].

[33] L. Hui, J. P. Ostriker, S. Tremaine, and E. Witten, "Ultralight scalars as cosmological dark matter," *Phys. Rev. D* **95** no. 4, (2017) 043541, arXiv:1610.08297 [astro-ph.CO].

[34] T. Kumar Poddar, S. Mohanty, and S. Jana, "Constraints on ultralight axions from compact binary systems," *Phys. Rev. D* **101** no. 8, (2020) 083007, arXiv:1906.00666 [hep-ph].

[35] T. K. Poddar and S. Mohanty, "Probing angle of birefringence due to long range axion hair from pulsars," arXiv:2003.11015 [hep-ph].

[36] T. Kumar Poddar, "Constraints on axionic fuzzy dark matter from light bending and Shapiro time delay," arXiv:2104.09772 [hep-ph].

[37] A. Boyarsky, M. Drewes, T. Lasserre, S. Mertens, and O. Ruchayskiy, "Sterile neutrino Dark Matter," *Prog. Part. Nucl. Phys.* **104** (2019) 1–45, arXiv:1807.07938 [hep-ph].

[38] B. Carr, F. Kuhnel, and M. Sandstad, "Primordial Black Holes as Dark Matter," *Phys. Rev. D* **94** no. 8, (2016) 083504, arXiv:1607.06077 [astro-ph.CO].

[39] B. C. Lacki and J. F. Beacom, "Primordial Black Holes as Dark Matter: Almost All or Almost Nothing," *Astrophys. J. Lett.* **720** (2010) L67–L71, arXiv:1003.3466 [astro-ph.CO].

[40] E. W. Kolb and M. S. Turner, *The Early Universe*, vol. 69. 1990.

[41] S. Mohanty, *Astroparticle Physics and Cosmology: Perspectives in the Multimessenger Era*, vol. 975. 2020.

[42] M. Shaposhnikov and I. Tkachev, "The nuMSM, inflation, and dark matter," *Phys. Lett. B* **639** (2006) 414–417, arXiv:hep-ph/0604236.

[43] K. Petraki and A. Kusenko, "Dark-matter sterile neutrinos in models with a gauge singlet in the Higgs sector," *Phys. Rev. D* **77** (2008) 065014, arXiv:0711.4646 [hep-ph].

[44] A. Abada, G. Arcadi, and M. Lucente, "Dark Matter in the minimal Inverse Seesaw mechanism," *JCAP* **10** (2014) 001, arXiv:1406.6556 [hep-ph].

[45] B. Shakya, "Sterile Neutrino Dark Matter from Freeze-In," *Mod. Phys. Lett. A* **31** no. 06, (2016) 1630005, arXiv:1512.02751 [hep-ph].

[46] M. Blennow, E. Fernandez-Martinez, and B. Zaldivar, "Freeze-in through portals," *JCAP* **01** (2014) 003, arXiv:1309.7348 [hep-ph].

[47] C. Cheung, G. Elor, L. J. Hall, and P. Kumar, "Origins of Hidden Sector Dark Matter I: Cosmology," *JHEP* **03** (2011) 042, arXiv:1010.0022 [hep-ph].

[48] F. Elahi, C. Kolda, and J. Unwin, "UltraViolet Freeze-in," *JHEP* **03** (2015) 048, arXiv:1410.6157 [hep-ph].

[49] J. McDonald, "Warm Dark Matter via Ultra-Violet Freeze-In: Reheating Temperature and Non-Thermal Distribution for Fermionic Higgs Portal Dark Matter," *JCAP* **08** (2016) 035, arXiv:1512.06422 [hep-ph].

[50] S.-L. Chen and Z. Kang, "On UltraViolet Freeze-in Dark Matter during Reheating," *JCAP* **05** (2018) 036, arXiv:1711.02556 [hep-ph].

[51] S. Alekhin *et al.*, "A facility to Search for Hidden Particles at the CERN SPS: the SHiP physics case," *Rept. Prog. Phys.* **79** no. 12, (2016) 124201, arXiv:1504.04855 [hep-ph].

[52] **FASER** Collaboration, A. Ariga *et al.*, "FASER's physics reach for long-lived particles," *Phys. Rev. D* **99** no. 9, (2019) 095011, arXiv:1811.12522 [hep-ph].

[53] **FASER** Collaboration, A. Ariga *et al.*, "FASER: ForwArd Search ExpeRiment at the LHC," arXiv:1901.04468 [hep-ex].

[54] J. Knodlseder *et al.*, "Early SPI / INTEGRAL contraints on the morphology of the 511 keV line emission in the 4th galactic quadrant," *Astron. Astrophys.* **411** (2003) L457–L460, arXiv:astro-ph/0309442.

[55] P. Jean *et al.*, "Early SPI / INTEGRAL measurements of 511 keV line emission from the 4th quadrant of the Galaxy," *Astron. Astrophys.* **407** (2003) L55, arXiv:astro-ph/0309484.

[56] N. Okada, S. Okada, and Q. Shafi, "Light Z and dark matter from $\mathrm{U}(1)_X$ gauge symmetry," *Phys. Lett. B* **810** (2020) 135845, arXiv:2003.02667 [hep-ph].

[57] W. Grimus and L. Lavoura, "The Seesaw mechanism at arbitrary order: Disentangling the small scale from the large scale," *JHEP* **11** (2000) 042, arXiv:hep-ph/0008179.

[58] Z.-z. Xing and S. Zhou, "Why is the 3 x 3 neutrino mixing matrix almost unitary in realistic seesaw models?," *HEPNP* **30** (2006) 828–832, arXiv:hep-ph/0512290.

[59] A. Abada and M. Lucente, "Looking for the minimal inverse seesaw realisation," *Nucl. Phys. B* **885** (2014) 651–678, arXiv:1401.1507 [hep-ph].

[60] I. Esteban, M. Gonzalez-Garcia, M. Maltoni, T. Schwetz, and A. Zhou, "The fate of hints: updated global analysis of three-flavor neutrino oscillations," *JHEP* **09** (2020) 178, arXiv:2007.14792 [hep-ph].

[61] *NuFIT 5.0*, 2020 (accessed on January 10, 2021). www.nu-fit.org.

[62] **Planck** Collaboration, N. Aghanim *et al.*, "Planck 2018 results. VI. Cosmological parameters," arXiv:1807.06209 [astro-ph.CO].

[63] S. Antusch and O. Fischer, "Probing the nonunitarity of the leptonic mixing matrix at the CEPC," arXiv:1604.00208 [hep-ph].

[64] **SINDRUM II** Collaboration, W. H. Bertl *et al.*, "A Search for muon to electron conversion in muonic gold," *Eur. Phys. J. C* **47** (2006) 337–346.

[65] R. Coy and M. Frigerio, "Effective approach to lepton observables: the seesaw case," *Phys. Rev. D* **99** no. 9, (2019) 095040, arXiv:1812.03165 [hep-ph].

[66] V. De Romeri, D. Karamitros, O. Lebedev, and T. Toma, "Neutrino dark matter and the Higgs portal: improved freeze-in analysis," *JHEP* **10** (2020) 137, arXiv:2003.12606 [hep-ph].

[67] **Fermi-LAT** Collaboration, M. Ackermann *et al.*, "Updated search for spectral lines from Galactic dark matter interactions with pass 8 data from the Fermi Large Area Telescope," *Phys. Rev. D* **91** no. 12, (2015) 122002, arXiv:1506.00013 [astro-ph.HE].

[68] R. Essig, E. Kuflik, S. D. McDermott, T. Volansky, and K. M. Zurek, "Constraining Light Dark Matter with Diffuse X-Ray and Gamma-Ray Observations," *JHEP* **11** (2013) 193, arXiv:1309.4091 [hep-ph].

[69] A. W. Strong, I. V. Moskalenko, and O. Reimer, "Diffuse galactic continuum gamma rays. A Model compatible with EGRET data and cosmic-ray measurements," *Astrophys. J.* **613** (2004) 962–976, arXiv:astro-ph/0406254.

[70] A. Boyarsky, D. Malyshev, A. Neronov, and O. Ruchayskiy, "Constraining DM properties with SPI," *Mon. Not. Roy. Astron. Soc.* **387** (2008) 1345, arXiv:0710.4922 [astro-ph].

[71] K. Perez, K. C. Y. Ng, J. F. Beacom, C. Hersh, S. Horiuchi, and R. Krivonos, "Almost closing the νMSM sterile neutrino dark matter window with NuSTAR," *Phys. Rev. D* **95** no. 12, (2017) 123002, arXiv:1609.00667 [astro-ph.HE].

[72] S. Riemer-Sorensen and S. H. Hansen, "Decaying dark matter in Draco," *Astron. Astrophys.* **500** (2009) L37–L40, arXiv:0901.2569 [astro-ph.CO].

[73] S. Horiuchi, P. J. Humphrey, J. Onorbe, K. N. Abazajian, M. Kaplinghat, and S. Garrison-Kimmel, "Sterile neutrino dark matter bounds from galaxies of the Local Group," *Phys. Rev. D* **89** no. 2, (2014) 025017, arXiv:1311.0282 [astro-ph.CO].

[74] M. Loewenstein, A. Kusenko, and P. L. Biermann, "New Limits on Sterile Neutrinos from Suzaku Observations of the Ursa Minor Dwarf Spheroidal Galaxy," *Astrophys. J.* **700** (2009) 426–435, arXiv:0812.2710 [astro-ph].

[75] C. R. Watson, J. F. Beacom, H. Yuksel, and T. P. Walker, "Direct X-ray Constraints on Sterile Neutrino Warm Dark Matter," *Phys. Rev. D* **74** (2006) 033009,

arXiv:astro-ph/0605424.

[76] H. Yuksel, J. F. Beacom, and C. R. Watson, "Strong Upper Limits on Sterile Neutrino Warm Dark Matter," *Phys. Rev. Lett.* **101** (2008) 121301, arXiv:0706.4084 [astro-ph].

[77] N. Mirabal, "Swift observation of Segue 1: constraints on sterile neutrino parameters in the darkest galaxy," *Mon. Not. Roy. Astron. Soc.* **409** (2010) 128, arXiv:1010.4706 [astro-ph.HE].

[78] B. M. Roach, K. C. Ng, K. Perez, J. F. Beacom, S. Horiuchi, R. Krivonos, and D. R. Wik, "NuSTAR Tests of Sterile-Neutrino Dark Matter: New Galactic Bulge Observations and Combined Impact," *Phys. Rev. D* **101** no. 10, (2020) 103011, arXiv:1908.09037 [astro-ph.HE].

[79] K. C. Y. Ng, S. Horiuchi, J. M. Gaskins, M. Smith, and R. Preece, "Improved Limits on Sterile Neutrino Dark Matter using Full-Sky Fermi Gamma-Ray Burst Monitor Data," *Phys. Rev. D* **92** no. 4, (2015) 043503, arXiv:1504.04027 [astro-ph.CO].

[80] T. R. Slatyer and C.-L. Wu, "General Constraints on Dark Matter Decay from the Cosmic Microwave Background," *Phys. Rev. D* **95** no. 2, (2017) 023010, arXiv:1610.06933 [astro-ph.CO].

[81] J. Casas and A. Ibarra, "Oscillating neutrinos and $\mu \to e, \gamma$," *Nucl. Phys. B* **618** (2001) 171–204, arXiv:hep-ph/0103065.

[82] M. J. Dolan, T. P. Dutka, and R. R. Volkas, "Dirac-Phase Thermal Leptogenesis in the extended Type-I Seesaw Model," *JCAP* **06** (2018) 012, arXiv:1802.08373 [hep-ph].

[83] K. Kannike, "Vacuum Stability Conditions From Copositivity Criteria," *Eur. Phys. J. C* **72** (2012) 2093, arXiv:1205.3781 [hep-ph].

[84] H. Huffel and G. Pocsik, "Unitarity Bounds on Higgs Boson Masses in the Weinberg-Salam Model With Two Higgs Doublets," *Z. Phys. C* **8** (1981) 13.

[85] M. Duerr, F. Kahlhoefer, K. Schmidt-Hoberg, T. Schwetz, and S. Vogl, "How to save the WIMP: global analysis of a dark matter model with two s-channel mediators," *JHEP* **09** (2016) 042, arXiv:1606.07609 [hep-ph].

[86] A. Sirlin and R. Zucchini, "Dependence of the Quartic Coupling H(m) on M(H) and the Possible Onset of New Physics in the Higgs Sector of the Standard Model," *Nucl. Phys. B*

266 (1986) 389–409.

[87] K. Melnikov and T. v. Ritbergen, "The Three loop relation between the MS-bar and the pole quark masses," *Phys. Lett. B* **482** (2000) 99–108, arXiv:hep-ph/9912391.

[88] M. Holthausen, K. S. Lim, and M. Lindner, "Planck scale Boundary Conditions and the Higgs Mass," *JHEP* **02** (2012) 037, arXiv:1112.2415 [hep-ph].

[89] F. Staub, "SARAH 4 : A tool for (not only SUSY) model builders," *Comput. Phys. Commun.* **185** (2014) 1773–1790, arXiv:1309.7223 [hep-ph].

[90] S. Alekhin, A. Djouadi, and S. Moch, "The top quark and Higgs boson masses and the stability of the electroweak vacuum," *Phys. Lett. B* **716** (2012) 214–219, arXiv:1207.0980 [hep-ph].

[91] D. Buttazzo, G. Degrassi, P. P. Giardino, G. F. Giudice, F. Sala, A. Salvio, and A. Strumia, "Investigating the near-criticality of the Higgs boson," *JHEP* **12** (2013) 089, arXiv:1307.3536 [hep-ph].

[92] I. Garg, S. Goswami, K. N. Vishnudath, and N. Khan, "Electroweak vacuum stability in presence of singlet scalar dark matter in TeV scale seesaw models," *Phys. Rev. D* **96** no. 5, (2017) 055020, arXiv:1706.08851 [hep-ph].

[93] B. W. Lee and S. Weinberg, "Cosmological Lower Bound on Heavy Neutrino Masses," *Phys. Rev. Lett.* **39** (1977) 165–168.

[94] S. Dodelson and L. M. Widrow, "Sterile-neutrinos as dark matter," *Phys. Rev. Lett.* **72** (1994) 17–20, arXiv:hep-ph/9303287.

[95] T. Asaka, M. Laine, and M. Shaposhnikov, "Lightest sterile neutrino abundance within the nuMSM," *JHEP* **01** (2007) 091, arXiv:hep-ph/0612182. [Erratum: JHEP 02, 028 (2015)].

[96] U. Seljak, A. Makarov, P. McDonald, and H. Trac, "Can sterile neutrinos be the dark matter?," *Phys. Rev. Lett.* **97** (2006) 191303, arXiv:astro-ph/0602430.

[97] A. Boyarsky, J. Lesgourgues, O. Ruchayskiy, and M. Viel, "Lyman-alpha constraints on warm and on warm-plus-cold dark matter models," *JCAP* **05** (2009) 012, arXiv:0812.0010 [astro-ph].

[98] X.-D. Shi and G. M. Fuller, "A New dark matter candidate: Nonthermal sterile neutrinos," *Phys. Rev. Lett.* **82** (1999) 2832–2835, arXiv:astro-ph/9810076.

[99] S. Horiuchi, B. Bozek, K. N. Abazajian, M. Boylan-Kolchin, J. S. Bullock, S. Garrison-Kimmel, and J. Onorbe, "Properties of resonantly produced sterile neutrino dark matter subhaloes," *Mon. Not. Roy. Astron. Soc.* **456** no. 4, (2016) 4346–4353, arXiv:1512.04548 [astro-ph.CO].

[100] A. Schneider, "Astrophysical constraints on resonantly produced sterile neutrino dark matter," *JCAP* **04** (2016) 059, arXiv:1601.07553 [astro-ph.CO].

[101] A. Kusenko, "Sterile neutrinos, dark matter, and the pulsar velocities in models with a Higgs singlet," *Phys. Rev. Lett.* **97** (2006) 241301, arXiv:hep-ph/0609081.

[102] H. Matsui and M. Nojiri, "Higgs sector extension of the neutrino minimal standard model with thermal freeze-in production mechanism," *Phys. Rev. D* **92** no. 2, (2015) 025045, arXiv:1503.01293 [hep-ph].

[103] **ATLAS** Collaboration, G. Aad *et al.*, "Search for high-mass dilepton resonances using 139 fb^{-1} of pp collision data collected at $\sqrt{s}$ =13 TeV with the ATLAS detector," *Phys. Lett. B* **796** (2019) 68–87, arXiv:1903.06248 [hep-ex].

[104] G. Raffelt, "Astrophysics probes of particle physics," *Phys. Rept.* **333** (2000) 593–618.

[105] J. Redondo and G. Raffelt, "Solar constraints on hidden photons re-visited," *JCAP* **08** (2013) 034, arXiv:1305.2920 [hep-ph].

[106] J. B. Dent, F. Ferrer, and L. M. Krauss, "Constraints on Light Hidden Sector Gauge Bosons from Supernova Cooling," arXiv:1201.2683 [astro-ph.CO].

[107] D. Kazanas, R. N. Mohapatra, S. Nussinov, V. L. Teplitz, and Y. Zhang, "Supernova Bounds on the Dark Photon Using its Electromagnetic Decay," *Nucl. Phys. B* **890** (2014) 17–29, arXiv:1410.0221 [hep-ph].

[108] G. Bellini *et al.*, "Precision measurement of the 7Be solar neutrino interaction rate in Borexino," *Phys. Rev. Lett.* **107** (2011) 141302, arXiv:1104.1816 [hep-ex].

[109] R. Harnik, J. Kopp, and P. A. Machado, "Exploring nu Signals in Dark Matter Detectors," *JCAP* **07** (2012) 026, arXiv:1202.6073 [hep-ph].

[110] M. Davier and H. Nguyen Ngoc, "An Unambiguous Search for a Light Higgs Boson," *Phys. Lett. B* **229** (1989) 150–155.

[111] J. Blümlein and J. Brunner, "New Exclusion Limits on Dark Gauge Forces from Proton Bremsstrahlung in Beam-Dump Data," *Phys. Lett. B* **731** (2014) 320–326, arXiv:1311.3870 [hep-ph].

[112] J. Bjorken, S. Ecklund, W. Nelson, A. Abashian, C. Church, B. Lu, L. Mo, T. Nunamaker, and P. Rassmann, "Search for Neutral Metastable Penetrating Particles Produced in the SLAC Beam Dump," *Phys. Rev. D* **38** (1988) 3375.

[113] D. Gorbunov, A. Makarov, and I. Timiryasov, "Decaying light particles in the SHiP experiment: Signal rate estimates for hidden photons," *Phys. Rev. D* **91** no. 3, (2015) 035027, arXiv:1411.4007 [hep-ph].

[114] J. L. Feng, I. Galon, F. Kling, and S. Trojanowski, "Dark Higgs bosons at the ForwArd Search ExpeRiment," *Phys. Rev. D* **97** no. 5, (2018) 055034, arXiv:1710.09387 [hep-ph].

[115] C. Boehm, D. Hooper, J. Silk, M. Casse, and J. Paul, "MeV dark matter: Has it been detected?," *Phys. Rev. Lett.* **92** (2004) 101301, arXiv:astro-ph/0309686.

[116] P. Fayet, "Light spin 1/2 or spin 0 dark matter particles," *Phys. Rev. D* **70** (2004) 023514, arXiv:hep-ph/0403226.

[117] J. F. Gunion, D. Hooper, and B. McElrath, "Light neutralino dark matter in the NMSSM," *Phys. Rev. D* **73** (2006) 015011, arXiv:hep-ph/0509024.

[118] C. Boehm, J. Orloff, and P. Salati, "Light Dark Matter Annihilations into Two Photons," *Phys. Lett. B* **641** (2006) 247–253, arXiv:astro-ph/0607437.

[119] D. Hooper and K. M. Zurek, "A Natural Supersymmetric Model with MeV Dark Matter," *Phys. Rev. D* **77** (2008) 087302, arXiv:0801.3686 [hep-ph].

[120] D. Hooper and L.-T. Wang, "Possible evidence for axino dark matter in the galactic bulge," *Phys. Rev. D* **70** (2004) 063506, arXiv:hep-ph/0402220.

[121] C. Picciotto and M. Pospelov, "Unstable relics as a source of galactic positrons," *Phys. Lett. B* **605** (2005) 15–25, arXiv:hep-ph/0402178.

[122] M. Kawasaki and T. Yanagida, "511-keV gamma ray from moduli decay in the galactic bluge," *Phys. Lett. B* **624** (2005) 162–165, arXiv:hep-ph/0505167.

[123] F. Takahashi and T. Yanagida, "Unification of dark energy and dark matter," *Phys. Lett. B* **635** (2006) 57–60, arXiv:hep-ph/0512296.

[124] S. Kasuya and F. Takahashi, "511-kev line from q balls in the galactic center," *Phys. Rev. D* **72** (2005) 085015, arXiv:astro-ph/0508391.

[125] M. Pospelov and A. Ritz, "The galactic 511 keV line from electroweak scale WIMPs," *Phys. Lett. B* **651** (2007) 208–215, arXiv:hep-ph/0703128.

[126] S. Kasuya and M. Kawasaki, "511 kev line and diffuse gamma rays from moduli," *Phys. Rev. D* **73** (2006) 063007, arXiv:astro-ph/0602296.

[127] E. J. Chun and H. B. Kim, "Axino Light Dark Matter and Neutrino Masses with R-parity Violation," *JHEP* **10** (2006) 082, arXiv:hep-ph/0607076.